Improved Microfabrication Technologies for Single Cell Metabolic Analysis

by

Ganquan Song

A Thesis Presented in Partial Fulfillment
of the Requirements for the Degree
Master of Science

Approved April 2014 by the
Graduate Supervisory Committee:

Deirdre R. Meldrum, Chair
Michael Goryll
Hong Wang
Yanqing Tian

ARIZONA STATE UNIVERSITY

May 2014

ABSTRACT

Within the last decade there has been remarkable interest in single-cell metabolic analysis as a key technology for understanding cellular heterogeneity, disease initiation, progression, and drug resistance. Technologies have been developed for oxygen consumption rate (OCR) measurements using various configurations of microfluidic devices. The technical challenges of current approaches include: (1) deposition of multiple sensors for multi-parameter metabolic measurements, e.g. oxygen, pH, etc.; (2) tedious and labor-intensive microwell array fabrication processes; (3) low yield of hermetic sealing between two rigid fused silica parts, even with a compliance layer of PDMS or Parylene-C.

In this thesis, several improved microfabrication technologies are developed and demonstrated for analyzing multiple metabolic parameters from single cells, including (1) a modified "lid-on-top" configuration with a multiple sensor trapping (MST) lid which spatially confines multiple sensors to micro-pockets enclosed by lips for hermetic sealing of wells; (2) a multiple step photo-polymerization method for patterning three optical sensors (oxygen, pH and reference) on fused silica and on a polyethylene terephthalate (PET) surface; (3) a photo-polymerization method for patterning tri-color (oxygen, pH and reference) optical sensors on both fused silica and on the PET surface; (4) improved KMPR/SU-8 microfabrication protocols for fabricating microwell arrays that can withstand cell culture conditions. Implementation of these improved microfabrication methods should address the aforementioned challenges and provide a high throughput and multi-parameter single cell metabolic analysis platform.

ACKNOWLEDGEMENTS

I would like to express my sincere gratitude to Arizona State University for letting me fulfill my dream of being a graduate student here. I would also like to thank the Center for Biosignatures Discovery Automation for giving me the opportunity to work on a very interesting project. To my committee, Dr. Deirdre Meldrum, Dr. Michael Goryll, Dr. Hong Wang, and Dr. Yanqing Tian, I am extremely grateful for your patient guidance and inspiring suggestions throughout my research. To Dr. Laimonas Kelbauskas and Benjamin Ueberroth, thank you for providing me an excellent station to operate the cell metabolic analysis and answering my endless questions. To Dr. Fengyu Su and Dr. Qian Mei, thank you for taking the beautiful confocal images of the magical sensors. To Dr. Liqiang Zhang and Dr. Xiangxing Kong, thank you for introducing me to the basic concepts of chemistry. To my teammates, especially Rishabh Shetty, and Arthur Wang, thank you for giving me words of encouragement and helping me fabricate complex devices. Most of all, I am fully indebted to Dr. Deirdre Meldrum, my advisor and director, for your understanding, patience, enthusiasm, wisdom, and encouragement and for pushing me farther than I thought I could go.

TABLE OF CONTENTS

Page

LIST OF TABLES

Table Page

LIST OF FIGURES

Figure Page

1. INTRODUCTION

1.1 Cell metabolism

Metabolism, a representative of all chemical reactions within an organism, is of tremendous interest in biochemical research applications with many fields to be explored [1]. Studies of cellular metabolic analysis developed over the past years have engendered a more far-reaching recognition of cellular metabolism. Depiction of metabolic pathways and their control apparatus, understanding of the kinetics and mechanism of enzymes involved, and explication of the structures are interrogated to reveal the function of cells and their influence on life decisions [2].

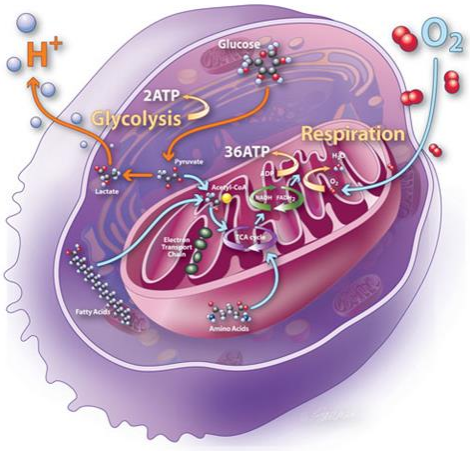

Figure 1: Cell metabolic pathways (Adapted from http://www.genengnews.com/gen-articles/advertorial-seahorse-bioscience/3867/)

Basically, every cell requires oxygen and nutrients to produce energy to perform cellular functions, such as mitosis, meiosis, glycolysis and fermentation. There are two primary pathways through which cells could acquire energy: lactic fermentation and aerobic respiration [3]. In the cytosol, glucose is converted from glycolysis to pyruvate, which is

subsequently reduced to lactate along with hydrogen ions and two ATPs. In the mitochondria, oxygen molecule functions as an electron accepter to create much higher energy when the pyruvate is oxidized in aerobic respiration. After these two processes, the direct results are the change of the extracellular concentration of oxygen and hydrogen ions, two key parameters to monitor the cellular metabolism.

1.1.1 The Warburg effect

One of the first breakthroughs for cancer studies was metabolic adaption in tumor cells. In the 1920s, Otto Warburg observed and announced that most cancer cells processed lactic fermentation in the cytosol to produce energy predominantly by a high rate of glycolysis, compared to the relatively low rate of glycolysis in mitochondria for most normal cells due to aerobic respiration [4]. Glycolytic rates in malignant tumor cells are up to 200 fold greater than those of normal cells. In another word, the metabolism of cancer cells is significantly different from that of normal cells, since cancer cells use glucose avidly but at the same time they only consume a small amount of oxygen for oxidative phosphorylation as respiration, even if the microenvironment has sufficient oxygen. According to this effect, the cancer cells tend to produce more hydrogen ions during the lactic fermentation and utilize less oxygen around the cells. Therefore, the two critical parameters, the extracellular concentration of oxygen and pH, reveal the significant difference between cancer cells and normal cells.

1.2 Bulk cell analysis v.s. single cell analysis

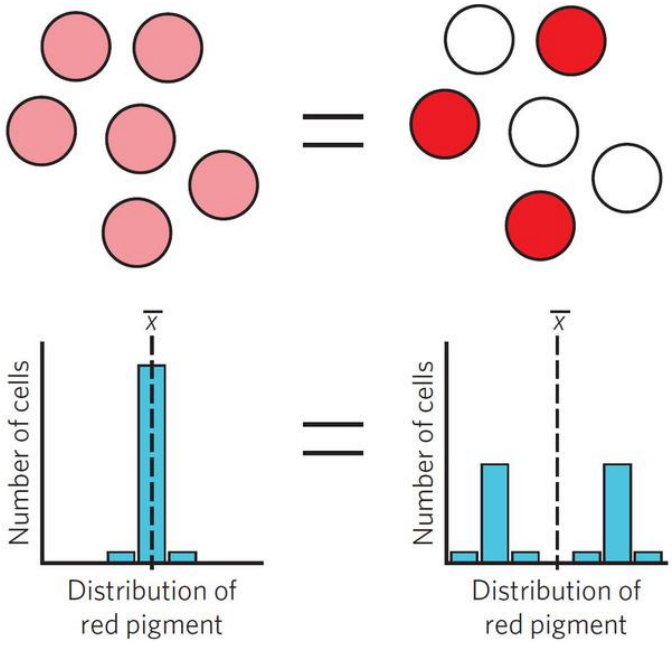

Figure 2: 'On'/ 'off' switch mechanism [5]

The cellular environment consists of a complex dynamic system with rapidly changing elements. Although it brings a lot of difficulties for cellular analysis, it provides a favorable platform for a system-level elucidation of how cells respond to extracellular perturbations [5]. Bulk cells analysis is not always accurate because cells responding to stimuli by distinct subpopulations are not a normal distribution, thus directly leading to (1) the impossibility of characterizing cell parameters at an intermediate state; (2) averaged out signals from a normal distribution. For instance, in a population average, if using pigment to describe bimodal distributions, the average value will lead to a complete wrong conclusion that there is no difference between a state with only pink cells and a state with half red cells and half white cells, although the distribution of the two state are

totally different (Figure 2). As well, minor subpopulations of cells could react to the external stimuli or environment change differently and then affect the rest of the population's behavior dramatically [5], leading to produce a substantial effect on the overall population. For example, there is only a small group of population showing growth response after perturbation while all the other matured cells stop responding or even die. When this small group of cells grows, they generate the same heterogeneity with the final population, but the averaged bulk result displays a growth response for all the cells. However, the actual mechanism is an immediate growth response rather than a growth lag in the whole population. Therefore, single cell analysis with high spatiotemporal resolution could provide nuanced understanding of cell-to-cell variations instead of the average output by bulk cell measurements. In summary, the effective way to measure the cellular heterogeneity is not the bulk cells, averaged measurements, which could blind researchers to mark the behavior of subpopulations and possibly interesting variations between cells.

1.3 Single cell analysis

The alternative way is single cell analysis (SCA), which is recognized as a key technology for understanding cellular heterogeneity in disease initiation and progression, and drug resistance [6]. Meanwhile heterogeneity among cell populations is a major factor in monitoring disease state of cells like cancer, and resistance to its treatment. Cellular heterogeneity is caused by stochasticity in the biological mechanism, which is the root of many metabolic processes [7]. Stochasticity, meaning random or lacking any

deterministic order, is a fundamental property of organic systems, because biochemical reactions have inherent random elements [8]. At the same time, cells do not share exactly the same size or same amount of important components. As mentioned in the previous example, bulk cells analysis would only achieve an averaged value when analyzing the bimodal distribution of a specific compound, and it tends to ignore the difference among individual cells. Therefore, analyzing individual cells could reveal the two different states of expression levels.

Investigating cancer cells is one of the most important applications of single cell analysis, because cancer tumors are not a group of identical cells characterizing the same properties [9]. For instance, genes expression such as proliferation may be inert in one region of cancer tumors but not in another. Or a minor population of tumor cells could dominate the phenotype, rendering them invisible and making the targeted therapy ineffective. The uncertain heterogeneity brings difficulty in describing the precise etiology and finding effective prescription for the disease. But through analyzing single cells interacting with their microenvironments, we have the ability to acquire information about particular cell lines. Critically it helps to understand how variations in cell phenotypes participate in the domination of functions by some cells over others through probing intercellular variability [10]. Therefore studies could demonstrate the mechanism of how cancer cells get away from the contact inhibition and plan out cells' life processes, including the impacts from external stimuli.

1.3.1 Challenges of single cell analysis

One major challenge for single cell analysis is to manipulate an integrated microsystem with micron scale objects. Usually the microsystem includes extremely complicated components of interest and is required to detect very small target amounts, causing difficulties in attaining adequate responses. Microfluidic or microfabrication systems (also known as 'lab-on-a-chip') have been proven as a promising method for single cell analysis, because they could combine the basic and inevitable processes about single cell analysis (such as selection, positioning or detection of target cells) [11]. The microfluidic devices provide the hermetic microchambers for analytes, which are isolated from the external microenvironments. These structures could keep them independent not influenced by their neighbors, so the detection can be accurate and reflect the actual mechanism [12].

Another challenge is to develop techniques to allow multiparameter analysis at the single cell level. Due to cell-to-cell heterogeneity, individual cells have different phenotypes and reflect different responses to the stimuli in the microenvironments. As a result, the reliable measurements of multiple appropriate parameters with high sensitivity and accuracy in a single cell will lead to a full understanding of the cellular specificity and complexity. Multiparameter analysis could provide new perspectives to reveal the information of intracellular mechanisms [13]. But currently most of the research is still in progress, and will be developed over the long term. To measure multiple various parameters at the same time, it requires analyzing single cells in a multiplexed fashion.

Moreover, the extremely rare amounts of materials used reveal small differential changes of metabolite concentrations especially from fragile cells, which make it more difficult to detect the multiple parameters by the limitation of the low signal-to-noise ratio.

1.3.2 Technologies for single cell analysis

Single cell analysis has been accomplished with a variety of techniques. Single fluorescence-activated cell sorting techniques provide a platform to monitor proteins or small molecules in living cells; and the reverse transcription-polymerase chain reaction helped to study single cell gene expression [14]. Single cell quantitative PCR and next generation sequencing are breakthrough technologies to realize single cell analysis, rather than by population based analysis. However, those techniques are often destructive to the cell, so that the final cellular response might be influenced by the invasive techniques rather than only by the perturbation. Therefore, these methods of single cell analysis cannot be used to follow the dynamic processes in undisturbed cells in real time (life on a chip).

The emergence of micro electro mechanical systems (MEMS) provides powerful technologies and miniaturized and integrated tools enabling single cell analysis with unprecedented sensitivity and specificity. MEMS refers to the fabrication of integrated systems with mechanical elements, sensors or actuators in the micrometer range [15]. Generally the related devices are made by the technique known as microfabrication.

In the 1950s, the invention of microtechnology opened new avenues for realizing integrated semiconductor structures for microelectronic chips [16]. Then pressure sensor manufacturing was achieved by lithography-based technologies in 1966 [17]. Along with further development of these technologies, MEMS started to include micrometer sized mechanical structures in silicon wafers. Afterwards, fluid-handling devices were introduced, including channels (capillary connections), mixers, valves, pumps, and dosing structures. In 1975, S. C. Terry proposed an analysis system with a gas chromatographic air integrated on a silicon wafer [18]. Next to this conception, research groups from Europe and North America developed micro-pumps, flow sensors and the ideas of integrated fluid treatments for analysis systems in the late 1980s and early 1990s. They also demonstrated that integration of pretreatment steps could apply the simple sensor functionality towards a complicated laboratory analysis [19]. An important breakthrough in research came in the 1990s, after the word Micro Total Analysis Systems (μTAS) was first coined by Andrew Manz in his foundation paper [20]. μTAS was also known as "lab-on-a-chip", referring to the micro-technologies that shrink an analytical or biochemical lab to a small footprint chip.

1.4 Previous approaches in the Center for Biosignatures Discovery Automation

The Center for Biosignatures Discovery Automation (CBDA) in the Biodesign Institute at Arizona State University and the NIH Center of Excellence in Genomic Sciences (CEGS) Microscale Life Sciences Center (MLSC), both directed by Professor Deirdre Meldrum, are focused on developing microscale technologies to analyze variations in

function at the single cell level and applying these technologies to fundamental problems of biology and healthcare (http://lifeonachip.org). The single cell metabolic profiling platform is one of the most powerful enabling tools developed in CBDA, which measures real-time concentrations of metabolic parameters of interest using extracellular fluorescence sensors hermetically sealed in microchambers containing single cells. The cell isolating microchambers are of sub-nanoliter volume, providing detection volumes that are sensitive to the concentration change of metabolites introduced by a single mammalian cell.

Different technical approaches for forming microchambers have been explored over the >10 years' development of metabolic profiling platforms.

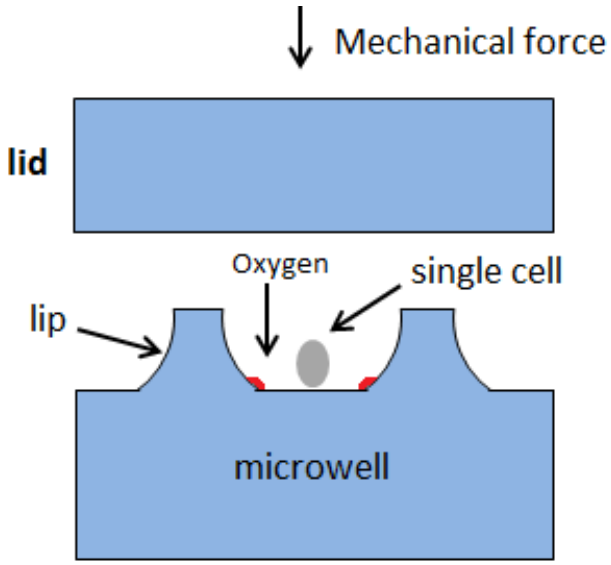

Figure 3: Microwells with oxygen sensors

In one of the initial approaches, oxygen consumption rate was measured by placing live cells in microwells containing oxygen sensors concentrated at the circumference of the microwell bottom (Figure 3: Microwells with oxygen sensors) [21]. A planar glass lid was pushed down on the top of microwells to form hermetical sealing that would isolate each microwell from the surrounding environment; oxygen cannot enter or leave the microwell. The oxygen concentration inside each of the microwells was measured in real time by an oxygen sensor, such as platinum (II) octaethylporphine (PtOEP). However, the major concerns of this approach are the potential chemical toxicity and/or photo toxicity highly reactive singlet oxygen species resulted from quenching of the triplet state of the sensors. Due to the vicinity of the sensor to the cells, these effects may interfere with cell function and other metabolic parameter measurements in a multiparameter metabolic profiling.

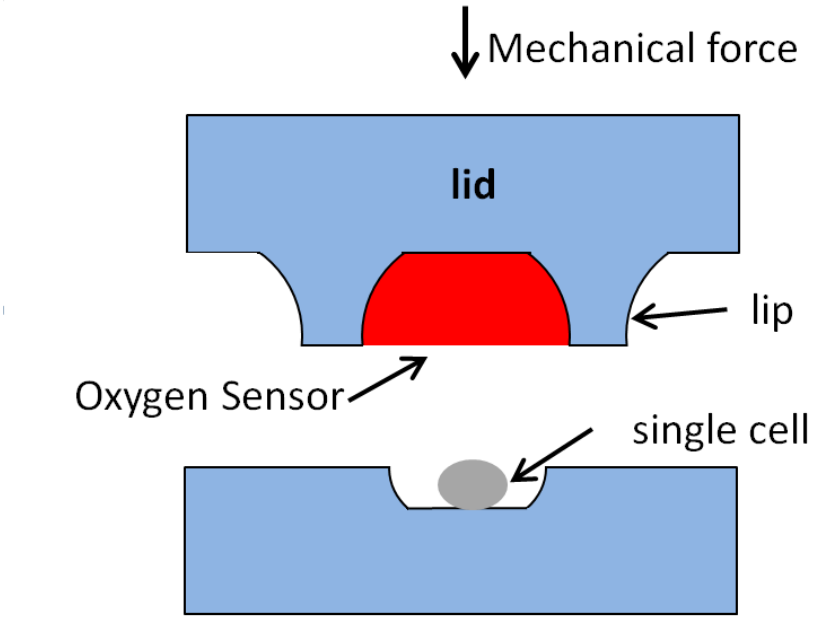

Figure 4: Microwell array configuration

In order to minimize the proximity effects from PtOEP sensors, a lid-on-top (LOT) design was developed (Figure 4) [22]. In this approach, hermetically sealed microchambers were formed by pressing a lid containing micropockets defined by lips for sensor deposition to a bottom chip containing microwells for single cell loading. This approach alleviates the stringent requirements of biocompatibility for sensors. In addition, compared to the seal between the planar surface and the microwell, a seal between the lips and microwells requires much less force and relaxes the requirements of surface flatness and particle-free contamination.

The most recent microchamber configuration consists of a "lip on bottom (LOB)" and a flat sensor film lid, which forms a hermetical seal. This approach provides significant progress in terms of throughput for the "Live-Cell Microarray for High-Throughput

Observation of Metabolic Signatures" project or Cellarium project, supported by the NIH common fund “Library of Integrated Network-based Cellular Signatures (LINCS)” program. The LOB is composed of 216 or, 1023 or 4095 microwells confined by lips for cell seeding (Figure 5). The lid is a tricolor sensor film made either by spin-coating (< 1 μm thickness) or by casting method (> 1 μm thickness). The advantages of this configuration include: (1) reducing the microfabrication hands-on time by ~40%. Only lips on the bottom need to be made using a wet-etching process, while the top flat sensor film is spin-coated or cast on a planar fused silica substrate. (2) No special setup is required for precise alignment between the sensor film top to LOB containing single cells, which is amenable to commercially available instruments. In CBDA, we use an off-the-shelf ImageXpress Micro (IXM) (Molecular Devices LLC, Sunnyvale, CA) and an in-house built manifold to perform high-throughput metabolic profiling assays.

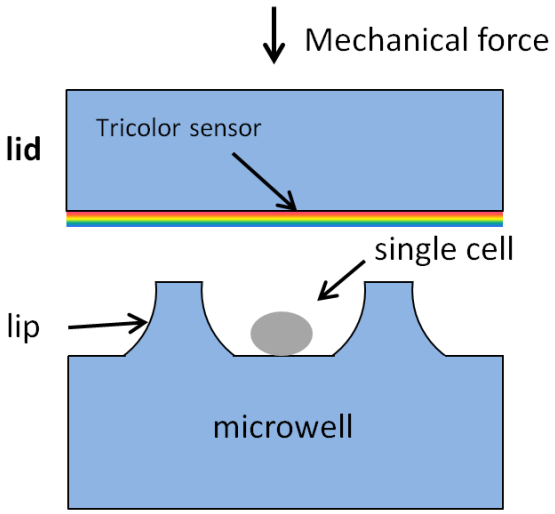

Figure 5: LOB configuration

In addition to oxygen, other metabolites, such as pH, glucose, carbon dioxide, ATP, etc., are also critical in metabolic profiling. Different approaches to extend the multiplexing capability of the metabolic measurement platform have been explored. One approach was to use multiple cycles of deposition, photoresist patterning and oxygen plasma etching to pattern two or more sensors of a variety of shapes and sizes. However, the performance of oxygen sensors was compromised due to the harsh plasma treatment conditions. Another approach is to fabricate multiple micro-pockets for accommodating different sensors as detailed in Chapter 2. The third approach is to develop multiple color sensors for measuring different metabolites.

1.5 Thesis summary

The technical challenges of current approaches include: (1) multiple sensor deposition for multi-parameter metabolic measurements, e.g. oxygen, pH, etc.; (2) tedious and labor-intensive microwell array fabrication process; (3) low yield of hermetic sealing between two rigid fused silica parts, even with a compliance layer of PDMS or Parylene-C.

In this thesis, several improved microfabrication technologies are demonstrated for analyzing multiple metabolic parameters from single cells, including (1) a modified "lid-on-top" configuration by developing a "multiple sensor top (MST) lid which spatially confines multiple sensors to micro-pockets enclosed by lips for hermetical sealing; (2) a multiple step photo-polymerization method for patterning three optical sensors (oxygen, pH and reference) on fused silica and on a polyethylene terephthalate (PET) surface; (3) a photo-polymerization method for patterning tri-color (oxygen, pH and reference) optical

sensors on both fused silica and on the PET surface; (4) improved KMPR/SU-8 microfabrication protocols for fabricating microwell arrays that can withstand cell culture conditions. By implementing these improved microfabrication methods, the aforementioned challenges should be addressed and should provide a high throughput and multi-parameter single cell metabolic analysis platform.

2. DESIGN, FABRICATION, AND CHARACTERIZATION OF MICRO-POCKET ARRAYS FOR MULTIPLE SENSOR TRAPPING (MST) LID

Ray et al. reported a platform for quantifying single cell oxygen consumption rates realized using a fused silica deep wet etching process [23]. In addition to oxygen, other metabolites, such as pH, glucose, carbon dioxide, ATP, etc., are also critical in metabolic profiling. In this chapter, this work is extended to a dual-depth wet etching process for microfabrication of multiple sensor trapping (MST) lid arrays. Each lid comprises multiple micro-pockets. Oxygen, pH, other extra-cellular sensors, and a reference dye were deposited in the pockets. In order to achieve simultaneous monitoring of multiple metabolic parameters, the lid array serves to hermetically seal arrays of microwells, each containing a single cell (Figure 6).

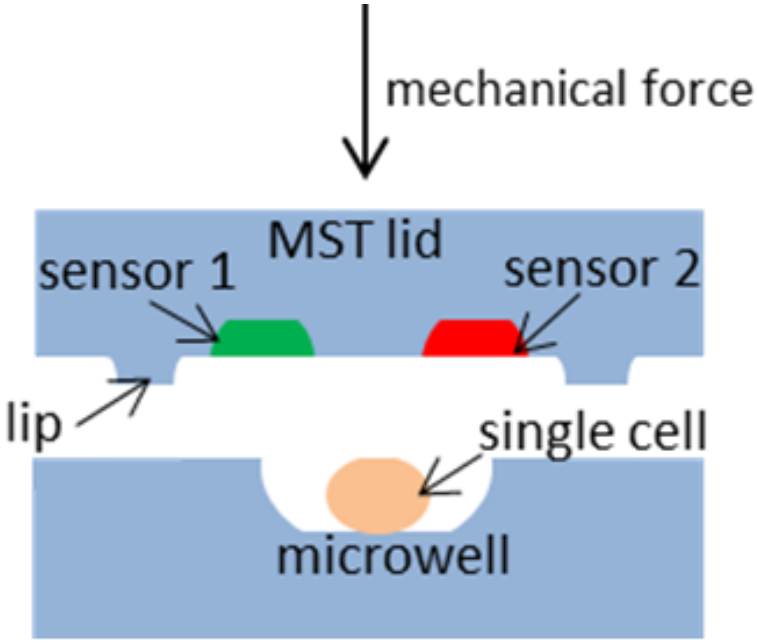

Figure 6: MST lid-on-Top configurations

2.1 Wafer level layout and chip design

The wafer layout for the MST lids and the bottom part for accommodating single cells are shown in Figure 7. The microwells for single cells were designed as to the final diameter of 50 µm to accommodating a single mammalian cell (10-20 µm diameter on average). The dimensions of micro-pockets were designed based on the preliminary experiments of sensor deposition. Undercut ratio of 1:1 of an isotropic wet etching was accounted for calculating the lateral dimensions in mask design. For example, to fabricate bottom microwells with a diameter of 50 µm and a depth of 10 µm, the corresponding circles on photomask must have a diameter of 30 µm.

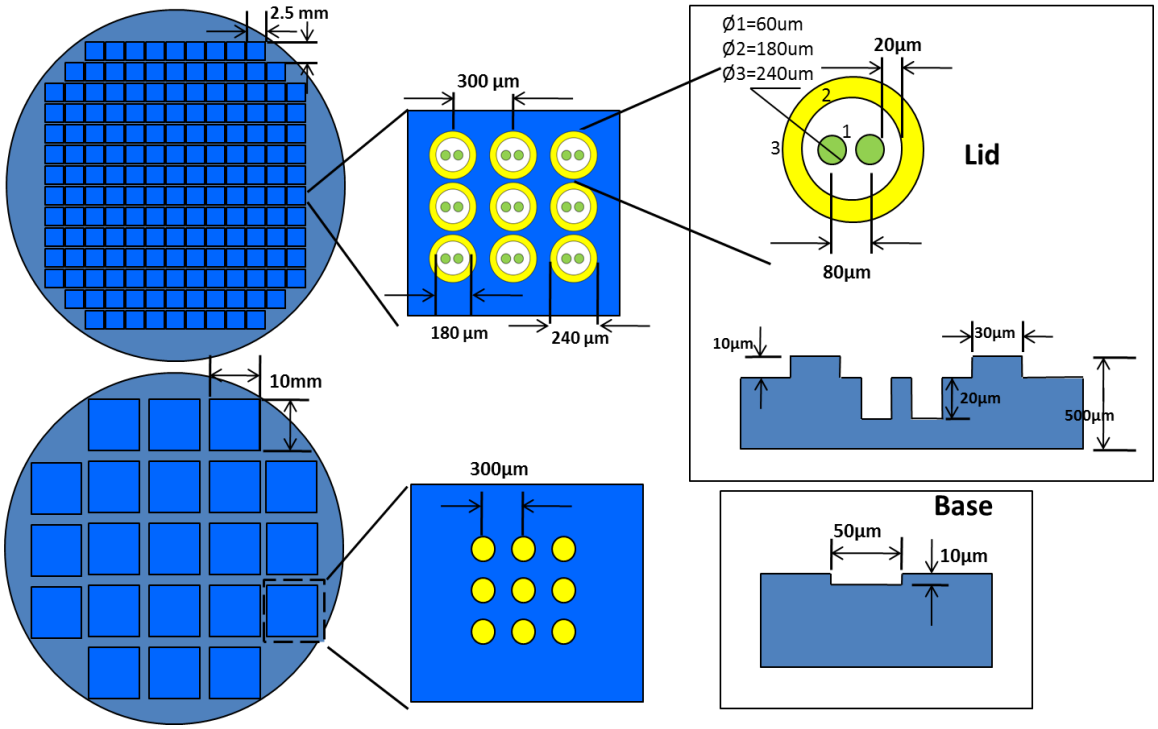

Figure 7: Wafer level layout for the dual-depth MST lid and bottom

2.2 Materials and chemicals

Four-inch double side polished fused silica wafers (University wafer, Boston, MA) were used as substrate material. AZ3312 or AZ 4620 Positive photoresists and AZ300MIF developer were purchased from Capital scientific, CA). Microstrip 2001 was purchased from Fujifilm. Photomasks were procured from Photoscience Inc. A mixture of 1 part ammonium hydroxide (27 wt%), 1 part hydrogen peroxide (30 wt%) and 5 parts DI water, and a mixture of 1 part hydrochloric acid (35 wt%), 1 part hydrogen peroxide (30 wt%) and 5 parts DI water were used for RCA 1 clean (base clean) and RCA 2 clean (acid clean), respectively. 49 wt% hydrofluoric acid was used to etch micro-wells into fused silica wafers. Trimethylsilylpropyl acrylate (TMSPA) was acquired from Sigma–Aldrich. We used platinum porphyrin derivative, Pt(II) Octaethylporphine (PtOEP, Frontier Scientific, Logan, UT) as the oxygen sensor. 1 mg PtOEP (O_2 sensor) was dissolved in 1 g of monomer ethyoxylated-(3)-trimethylolpropane triacrylate (SR454, Sartomer, Exton, PA) solution containing 10 mg azobisisobutyronitrile (AIBN, Sigma-Aldrich, St. Louis, MO). AIBN was used as a thermal initiator of free radical polymerization of SR454. The mixture was sonicated until a homogenous solution was obtained and then stored at 4 °C until use. The formulations of pH sensors (S1 and S2) were previously published [4, 8]: Briefly, 1 mg of the monomeric a naphthalimide derived S1 or fluorescein-derived S2, 800 mg of 2-hydroxyethyl methacrylate, 150 mg of acrylamide, 50 mg of SR454, and 10 mg of AIBN were dissolved in 1 mL DMF as a stock solution.

2.3 Microfabrication techniques and process flow

The schematic representation for the fabrication of top dual-pocket lids is shown in Figure 8. The process flow is shown in Table 1.

Table 1: Detailed process flow of the fabrication of top dual-pocket lid

Important Steps	Dual-Pocket Well Microfabrication Procedure
RCA cleaning	▪ RCA 1: 1250mL DI water, 250mL NH_4OH and 250mL H_2O_2 at 75°C for 10minutes ▪ RCA 2: 1200mL DI water, 200mL HCl and 200mL H_2O_2 at 75°C for 10minutes ▪ Thorough rinse with DI water (2 cycles) ▪ Dry with Nitrogen blow
a-Si coating	▪ 100sccm SiH_4 atmosphere ▪ 250 mTorr pressure ▪ 550 °C
AZ 4330 Process	▪ Apply HDMS ▪ Spin speed 4500 rpm ▪ Softbake at 90°C for 90 seconds ▪ Exposure 150 mJ/cm^2 ▪ AZ300MIF dip developing ▪ Develop for 60 ~ 90 seconds ▪ Rinse in DI water and then dry with Nitrogen blow ▪ Hardbake at 110°C for 3 minutes

First a-Si etch (Substrate)	▪ RIE dry etch recipe: 50sccm CF_4, 5sccm O_2, 100mT, 100W ▪ Etch time: 10 minutes
Second a-Si etch (Substrate Front)	▪ RIE dry etch recipe: 50sccm CF_4, 5sccm O_2, 100mT, 100W ▪ Etch time: 8.5 minutes
First HF wet etch	▪ 300mL 49% HF acid at room temperature ▪ Etch time: around 14 ~ 15 minutes (inspection required) ▪ Etch depth: 20um ± 1um
AZ 4330 Process	▪ Apply HDMS ▪ Spin speed 4500 rpm ▪ Softbake at 90°C for 90 seconds ▪ Proper alignment required by alignment marks ▪ Exposure 150 mJ/cm^2 ▪ AZ300MIF dip developing ▪ Develop for 60 ~ 90 seconds ▪ Rinse in DI water and then dry with Nitrogen blow ▪ ADI pattern check ▪ Hardbake at 110°C for 3 minutes
Third a-Si etch	Exactly same with the second a-Si etch process
Second HF wet etch	▪ 300mL 49% HF acid at room temperature ▪ Etch time: around 7 ~ 8 minutes (inspection required) ▪ Etch depth: 10um ± 1um
Last a-Si etch	Exactly same with the first a-Si etch process

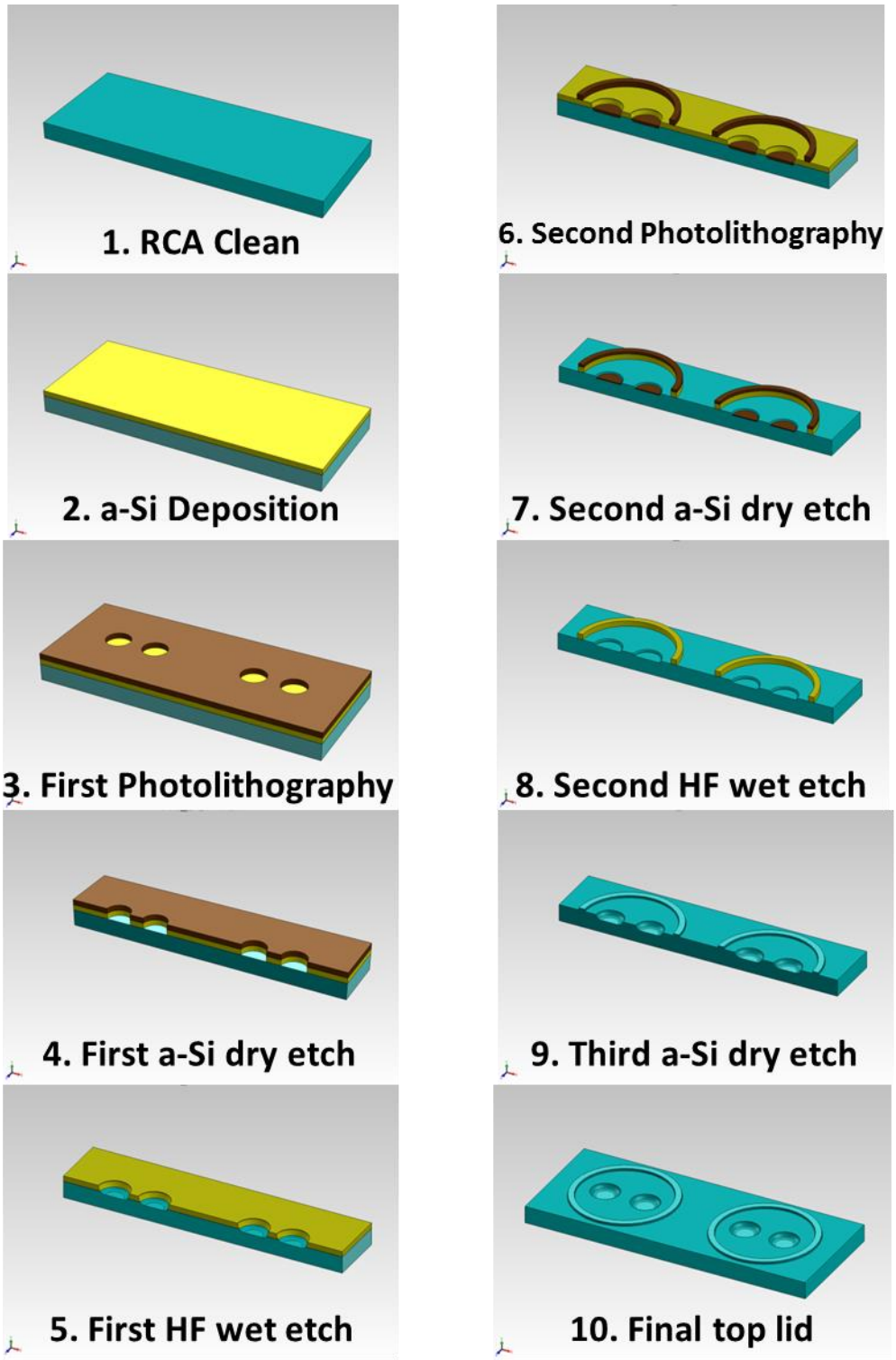

Figure 8: A schematic representation of fabrication process flow for MST lids

The fabrication of the bottom microwell for single cell attachment used similar procedures. Instead of using a two-step process, a single step process of photolithography, RIE dry etch and HF wet etch was used to create microwells of 50 μm diameter and 10 μm depth. The wafer was then diced to 13 x 13 mm dies for cell loading.

2.4 Sensor deposition

The surface of the MST lids was activated by 5 min oxygen plasma treatment (Harrick PDC-32G), followed by overnight vapor salinization using TMSPA. Different sensors, such as platinum porphyrin derivative (PtOEP) oxygen sensor or fluorescein derivative pH sensor, were mixed with 2-hydroxyethyl methacrylate solution and then deposited into separate micro-pockets using a noncontact piezoelectric liquid dispenser. The sensor solutions in the micro-pockets were thermally cured for 3 hours at 80°C under nitrogen atmosphere.

2.5 Results and discussions

2.5.1 Microfabrication

Fused silica is a very attractive material for metabolic analysis in microdevice fabrication: 1) its superior optical properties are compatible with highly sensitive fluorescence measurement; 2) its high purity (~100% silicon dioxide) minimizes non-uniformity and defects which ensures hermetic sealing for oxygen consumption measurements; 3) it is affordable compared with fused or crystal quartz. Previously reported fused silica microfabrication procedures that combine plasma dry etch and HF wet etching are

reported in [24],[23]. In this thesis, dual depth microstructure fabrication procedures are developed.

Figure 2.4 shows a 3-D optical profile of 5 x 5 arrays of dual pockets lids with a pitch of 300 µm. The dual 60 µm diameter pockets were enclosed by the lip with the inner diameter of 180 µm and the outer diameter is 240 µm. The depths of the dual pockets and lips were designed as 20 µm and 10 µm and measured 19.3 µm (Figure 9 a) and 9.5 µm (Figure 9 b) after fabrication, respectively.

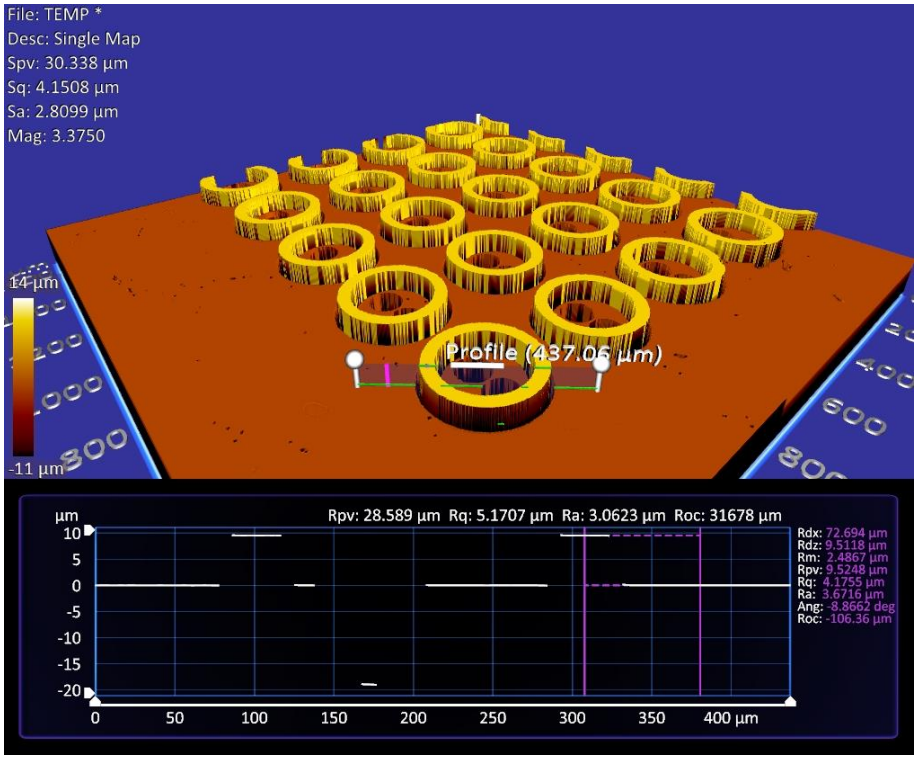

(a)

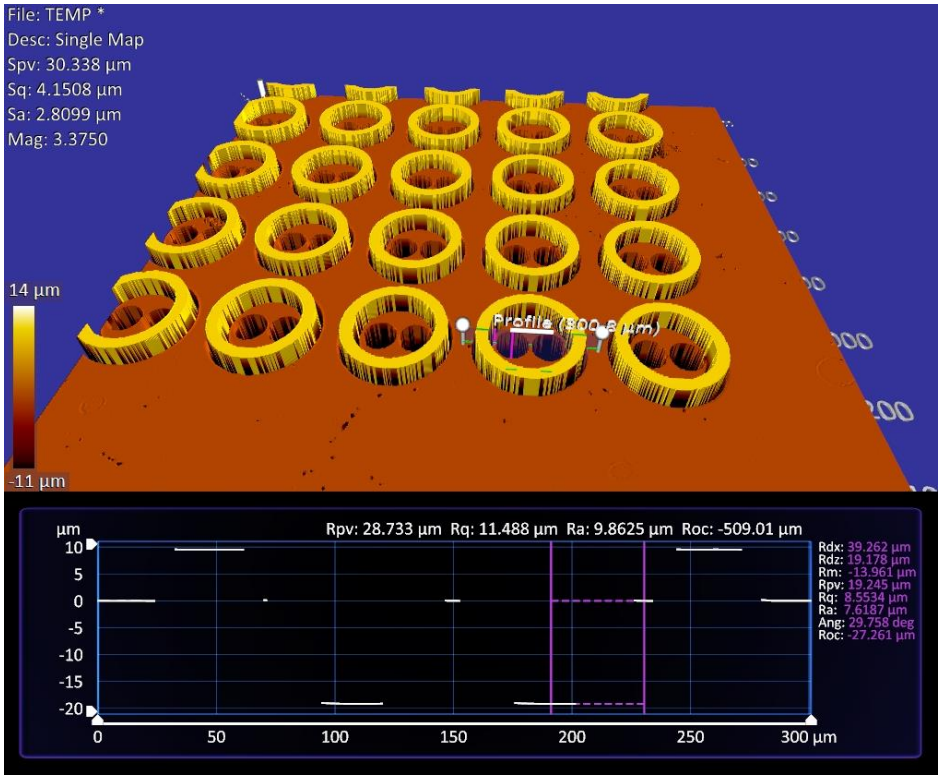

(b)

Figure 9: Optical profiler images showing the diameter and depth (b) micro-pockets surrounded by (a) lips

An SEM image in Figure 10 shows a laser scribed cross-section consisting of two pockets for different sensors.

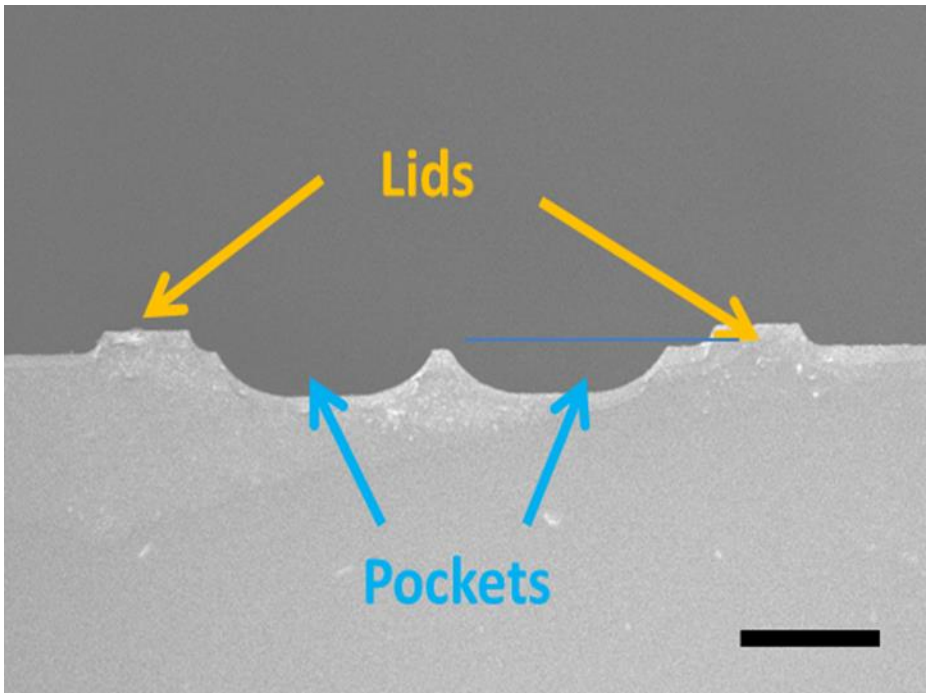

Figure 10: Cross-sectional SEM image of a dual-pocket lid (Scale bar: 50 µm)

Figure 11 shows the bottom microwell with 300 µm matching the top lids. The diameter of each microwell was 50 µm and the depth was 10 µm designed for single cell loading and incubation. The top lids and bottom microwell could be aligned and hermetically sealed for single cell metabolic analysis as shown in Figure 12.

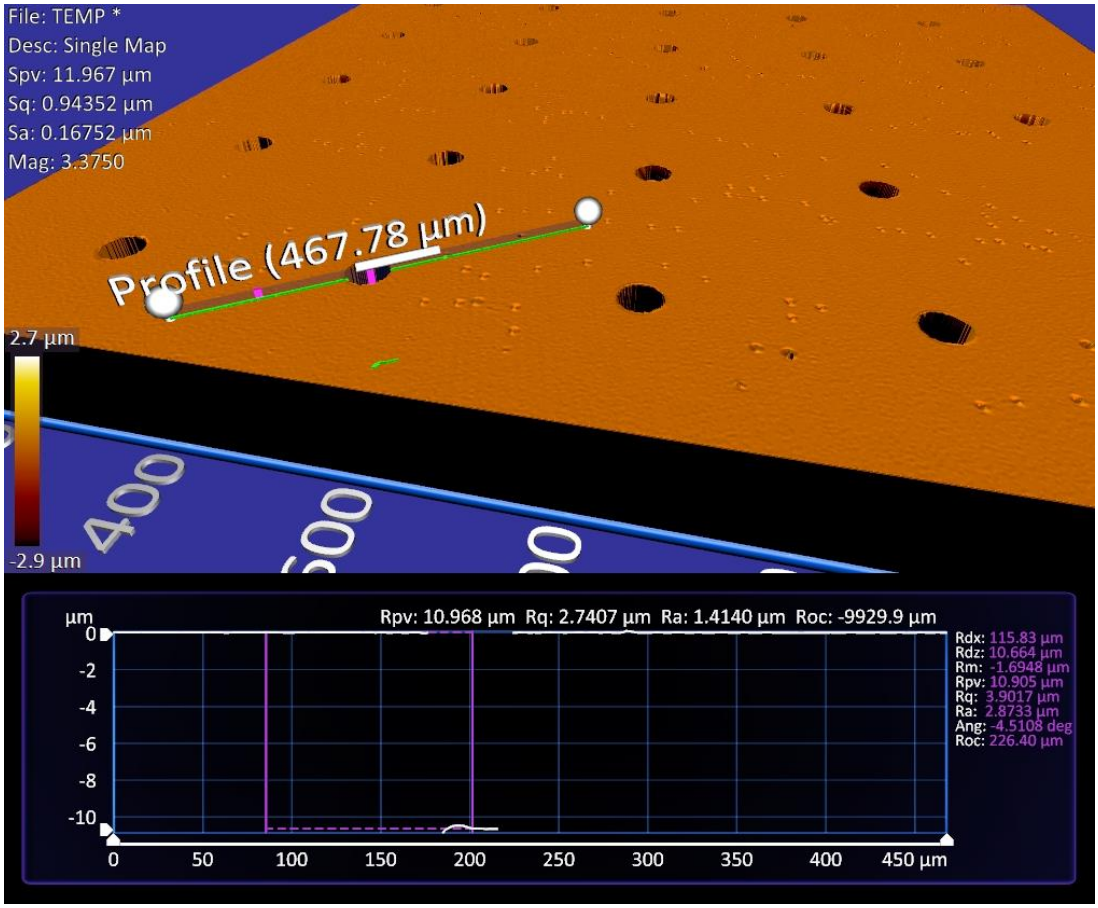

Figure 11: Optical profiler image for bottom die

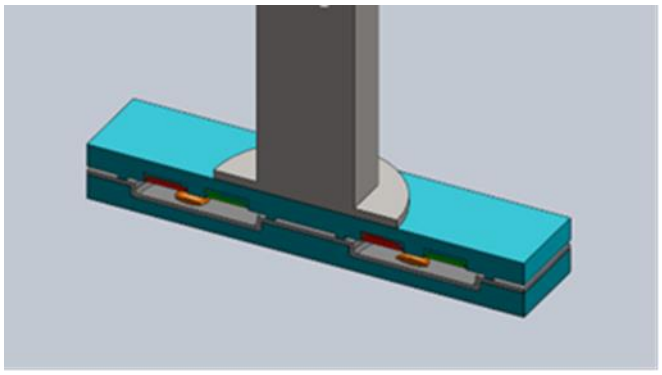

Figure 12: Schematic representation of the hermetic seal between the MST lid and microwell bottom

2.5.2 Etching depth variations

It is critical to have the same microchamber volume for metabolic measurements, such as oxygen consumption rate. Therefore, the etch uniformity across the whole wafer is one of the most important parameters in wet-etch process development. The height of the lids was measured across the central line of a 4 inch wafer using a contact stylus profiler (Dektak 150, Veeco, Tucson, AZ) and the results were plotted in Figure 13. The lids located on the edge of the wafer were slightly higher than those located on the center of the wafer, which indicated a higher etch rate at the edge. However, the difference was only about 0.1 μm for 10 μm etch, resulting in negligible variations (~1%) in volume related metabolic measurements.

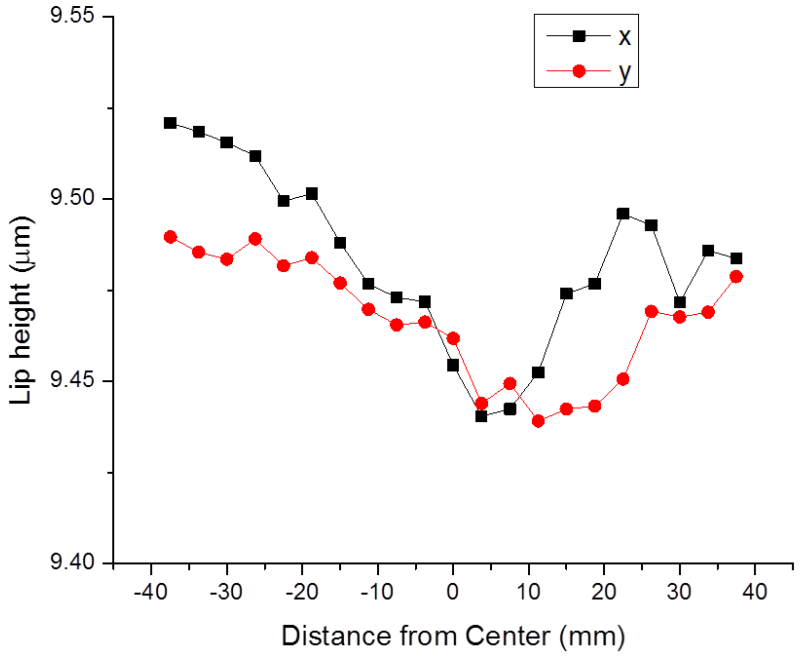

Figure 13: Etching depth across the 4 inch wafer

2.5.3 Surface roughness

The surface roughness after HF wet etch is also critical for precise microchamber volume control. High surface roughness will reduce optical clearance and lead to a high background fluorescent signal. The fused silica wafers were scanned using an AFM with scanasyst-air tips (Bruker, Inc.). The average surface roughness before and after a 10 µm etch was 2.52 nm and 5.43 nm, respectively (Figure 14). The low surface roughness can be attributed to the high purity of fused silica (no local mask effects from impurities).

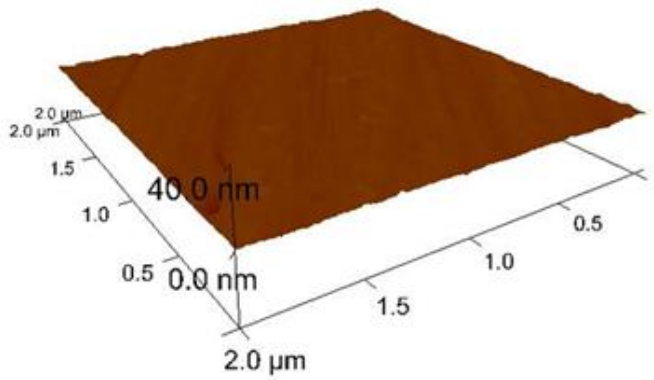

(a)

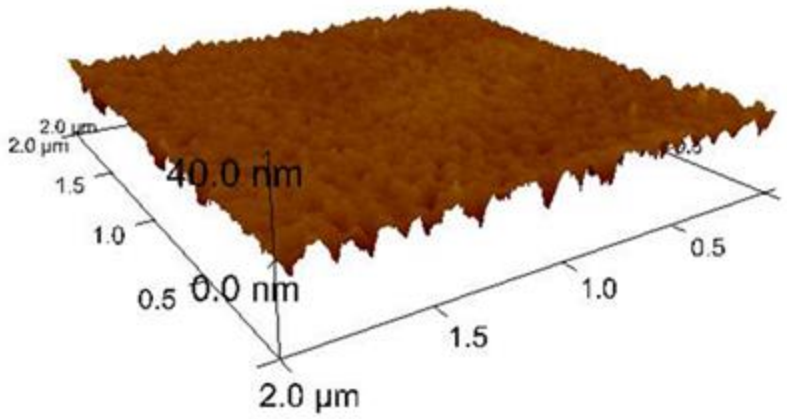

(b)

Figure 14: AFM image of fused silica surface (a) before and (b) after HF etch

2.5.4 Sensor characterization

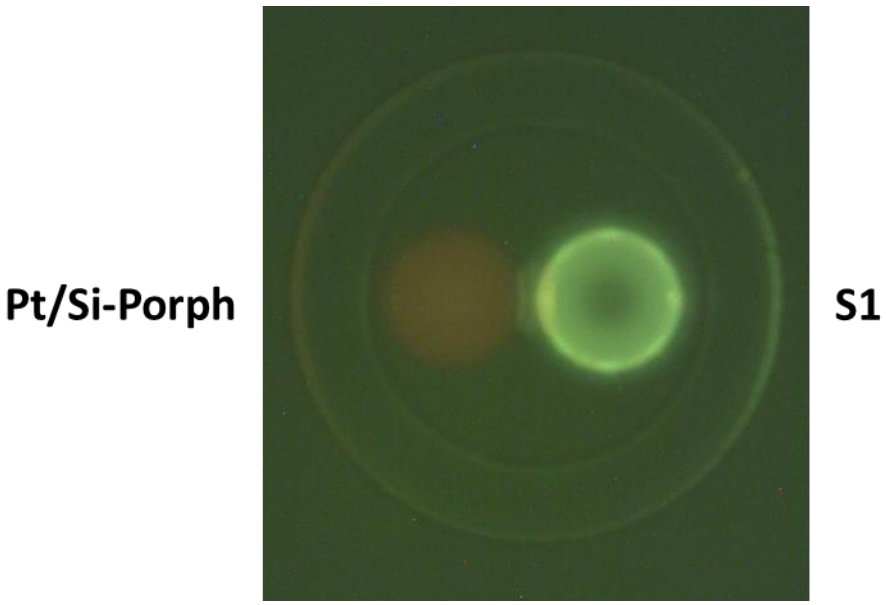

Figure 15: Fluorescence micrographs of a dual micro-pocket MST lid

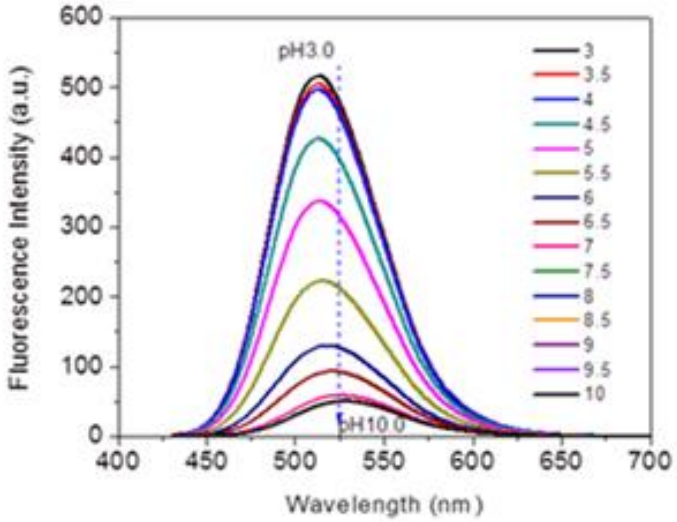

(a)

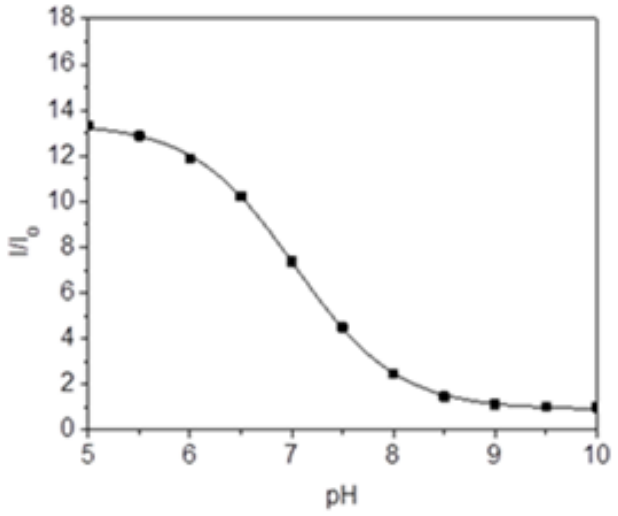

(b)

Figure 16: (a) pH responses of S1 film. Changes of fluorescence by pH at an excitation wavelength of 405 nm; b) fluorescence intensity (at 520 nm) ratios from pH 10 to pH 5; I is the fluorescence intensity at various pH; I0 is the fluorescence intensity at pH 10

Figure 15 shows typical fluorescence micrographs of a dual pocket MST lid. Fluorescence micrographs of an eight-pocket lid containing four different sensors are shown in Figure 16 (a). The sensors in thin film states were characterized using a spectrofluorophotometer under the sensors' suitable excitation wavelengths. S1 was excited at 405 nm. S2 was excited at 488 nm. PtOEP was excited at 380 nm. Figure 16 (b) shows the typical responses of the pH sensor S1. The emission intensity increased with a decrease in pH values. Emission intensity changes and the Boltzmann fitting of the sensor are given in Figure 16 (b). Results showed that pKa value of the sensor S1 is 7.0, indicating that the sensor is suitable for biological application.

2.6 Summary

In summary, MST lid arrays were designed and fabricated on fused silica substrate for accommodating multiple sensors for multiparameter metabolic analysis. A two-step photolithography and wet etching process was successfully applied to fabricate dual depth microstructures with high uniformity and low surface roughness. The demonstration of multiple spatially resolved sensors in MST lids provides a foundation for multiparameter analysis of cell respiration and other metabolic parameters at the single-cell, multiple-cell, and tissue level.

3. PHOTO-PATTERNED, MULTIPLEXED FLUORESCENCE SENSOR ARRAYS FOR SINGLE CELL MULTI-PARAMETER METABOLIC PROFILING

In Chapter 2, MST lids were developed for multi-parameter single cell metabolic analysis. However, the dual-step wet etching process is labor intensive and time consuming. In addition, the minimum diameter and thus the volume of the microchamber for accommodating multiple micro-pockets are limited by two factors: (1) the minimal micro-pocket volume to circumvent the overflow of the solution during deposition; (2) the intrinsic physics of 1:1 undercut from the wet etching process. The minimal diameter of a dual micro-pocket chamber is >150 μm. The relative large volume microchambers are suitable for metabolic profiling of >10-100 cells instead of single cells. In this chapter, the photo-patterning of photo polymerizable sensors on the fused silica surface are investigated and its applications in single cell metabolic profiling are demonstrated.

3.1 Materials and instrument

Trimethylsilylpropyl acrylate (TMSPA) and (Tridecafluoro-1,1,2,2-tetrahydrooctyl)-1-trichlorosilane were acquired from Sigma–Aldrich (St. Louis, MO). AZ4330 positive photoresists, AZ300MIF developer and chromium etchants (mixtures of perchloric acid and ceric ammonium nitrate) were supplied by the Center for Solid State Electronics Research (CSSER), Arizona State University, Tempe, AZ. Four-inch double-sided polished fused silica wafers were purchased from the University Wafer (South Boston, MA). RCA 1 (base clean), RCA 2 (acid clean) and HF were prepared as detailed in Chapter 2.

A polymerizable pH and oxygen non-responsive reference, a polymerizable fluorescein-derived pH sensor and a polymerizable platinum prophyrin-derived oxygen sensor were synthesized by the chemistry group led by Dr. Yanqing Tian in CBDA.

A spin coater (P-6708, Specialty Coating Systems, Indianapolis, IN), hotplate (Model 1000-1, Electronic Micro Systems Ltd., Wiltshire) and UV mask aligners (OAI-200 and OAI-808, OAI, San Jose, CA) were used for standard photolithography process.

Maskless Photolithography System (SF-100, Intelligent Micro patterning LLC, St. Petersburg, FL) was used in photo-patterning polymerizable sensors mixed with photoinitiator. Filter sets with peak wavelengths of 380 nm, 405 nm and 435 nm were studied for photo-patterning.

The optical microscope (LV150, Nikon, Melville, NY), equipped with a QIClick CCD camera (Model QIClick-F-M-12, QImaging, Surrey, BC), was used to visualize the feature surface and measure the dimensions of the micro-pattern. Dektak 150 stylus contact profiler (Veeco, Tuscon, AZ) was used to characterize the substrate surface and measure the thickness of the sensor spots. Eclipse TE2000E Nikon confocal fluorescence microscope (Melville, NY) was used for fluorescence imaging. Fused silica wafers were diced to squares of 13 mm dies using DISCO Automation Dicing Saw (DAD3220, Santa Clara, CA) for sensor photo-patterning. A spectrofluorophotometer (RF 5301, Shimadzu Scientific Instruments, Columbia, MD) was used to record responses of sensors.

3.2 Photo-patterning process

The photo-patterning process was performed using a SF-100 Maskless Photolithography

System (MPS), which is driven by a Digital Micromirror Device (DMD) manufactured by Texas Instruments. SF-100 can perform the photolithography process without the need for expensive photo-masks. It combines optical, electric and software components to project a virtual mask onto the surface of a flat substrate or non-flat surface, such as the bottom of microwells surrounded by the lips as shown in Chapter 2.

The fabrication procedure is represented in Figure 17. Briefly, fused silica dies with chrome L-markers for alignment were activated by oxygen plasma and functionalized by 3-acryloxypropyl trimethoxysilane. Three AutoCAD visual masks were used to sequentially photo-polymerize references, pH sensors, and oxygen sensors.

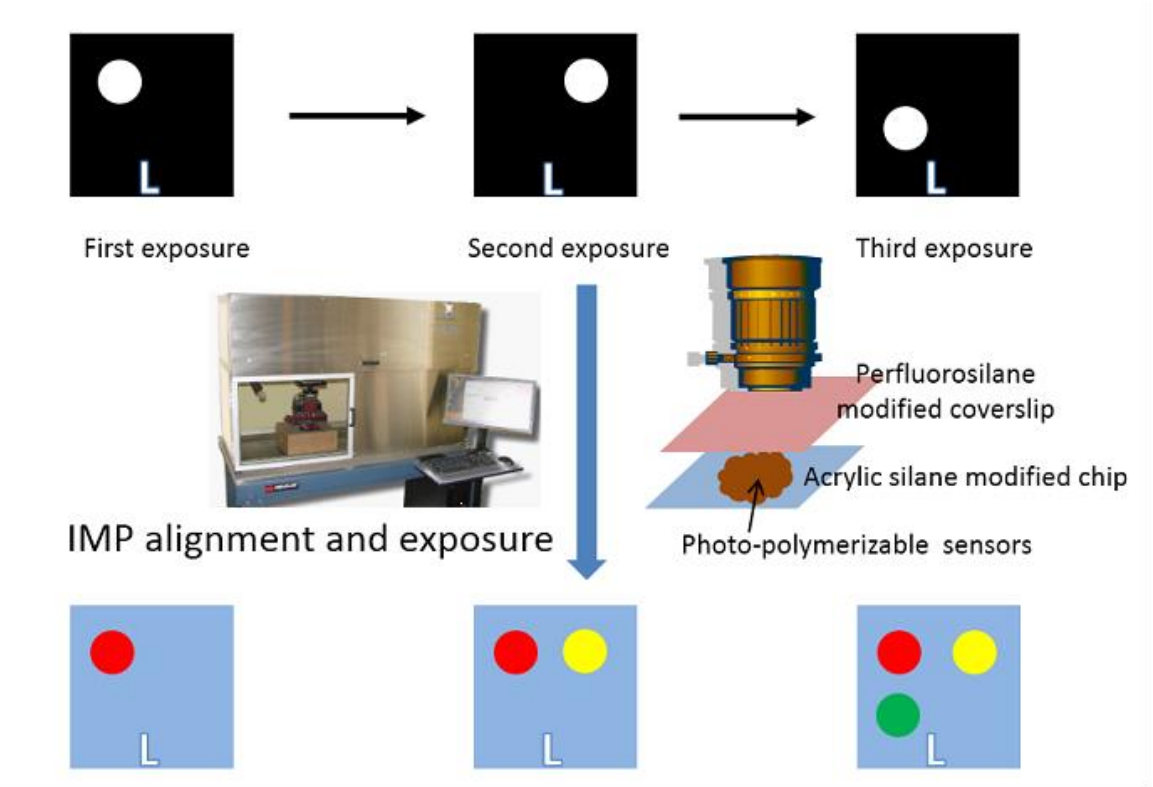

Figure 17: Schematic representation of multi-step photo-polymerization process for patterning three fluorescence sensors

Each of the visual masks has the same L-marker as that on fused silica die, which was used to align three sensors during the multi-step exposure process. 3 x 3 arrays of triple sensors were photo-patterned with 300 μm pitch. Three different sensor spots, each of a diameter of 20 μm, were confined in a 90 μm diameter circle. Typical fluorescence images collected using three sets of fluorescence filters and the bright field image of polymerized sensors are shown in Figure 18.

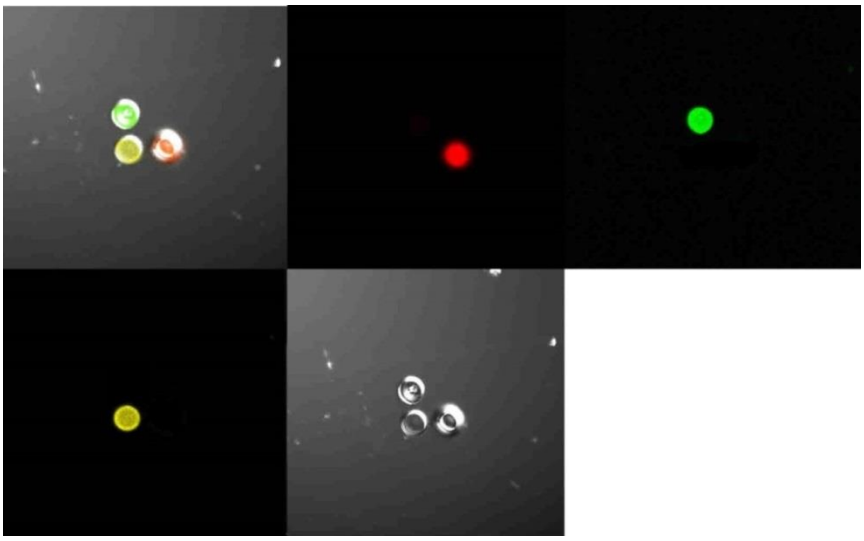

Figure 18: Fluorescence images collected using three sets of filters and the bright field image of photo-polymerized sensors

3.3 Results and discussions

3.3.1 Sensor responses

3.3.1.1 pH sensor responses

Figure 19 (a) shows the pH responses of a pH sensor film excited at 488 nm. Its emission intensity with a maximum at 515 nm increases with the increase of pH value. Figure 19 (b) shows the ratios of the fluorescence intensities at 515 nm at different pH values. It can

be found that the fluorescence intensity ratios changed about 175 fold from pH 3 to pH 9, indicating its exceptionally high sensitivity to pH. The sensor has a pKa of 7.1, showing that the sensor is suitable for biological applications. The intramolecular charge transfer and tautomerization of the fluorescein group in the pH sensor results in the pH responses.

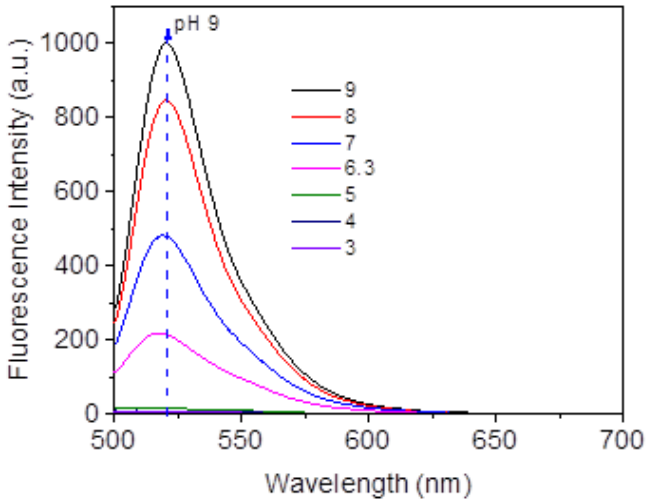

(a)

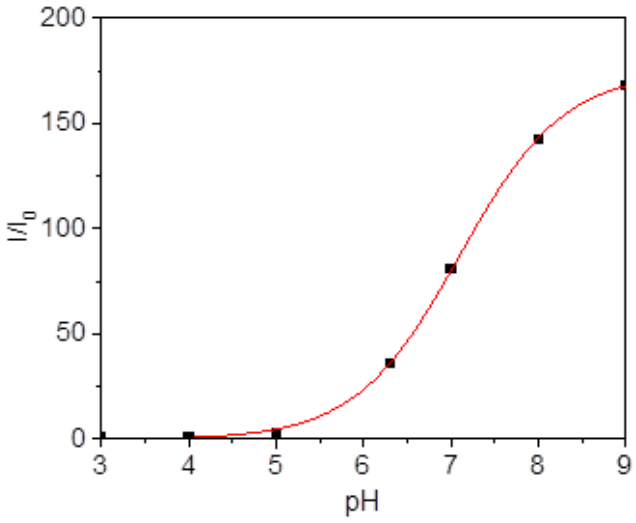

(b)

Figure 19: pH responses of the pH sensor film excited at 488 nm; (b) pH responses as measured using emission intensity at 515 nm; I is the intensity at 515 nm. I0 is the intensity at 515 nm at pH=3

3.3.1.2 Oxygen sensor responses

Figure 20 (a) shows the oxygen responses of the oxygen sensor film. Figure 20 (b) shows the Stern-Volmer plot of the sensor at different dissolved oxygen concentration. Similar with other oxygen sensor films using the same oxygen probe, a linear Stern-Volmer plot was observed.

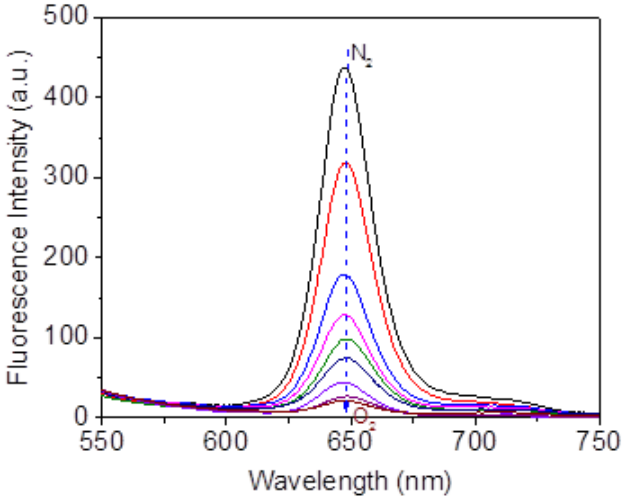

(a)

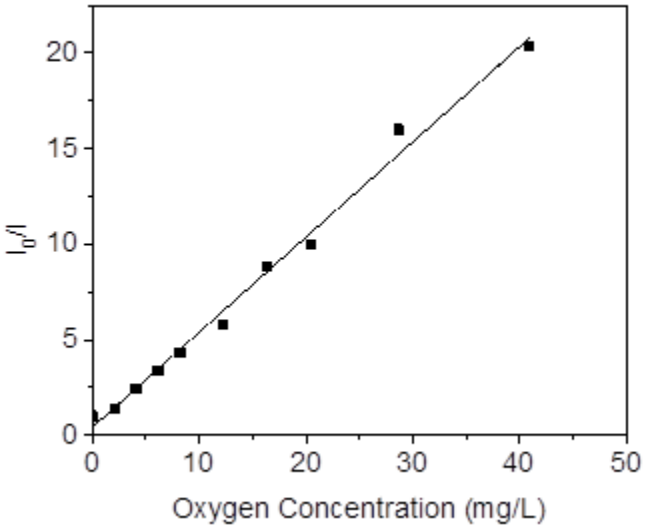

(b)

Figure 20: (a) The oxygen responses of the oxygen sensor film; (b) The Stern-Volmer plot of the oxygen sensor at different dissolved oxygen concentration

3.3.1.3 Spectral characterization of the reference probe

Figure 21 (a) and (b) show the fluorescence intensity of the reference probe at different pH and different oxygen concentrations, respectively. The results indicate that the

reference probe is not responsive to pH or oxygen concentrations, which is an ideal result.

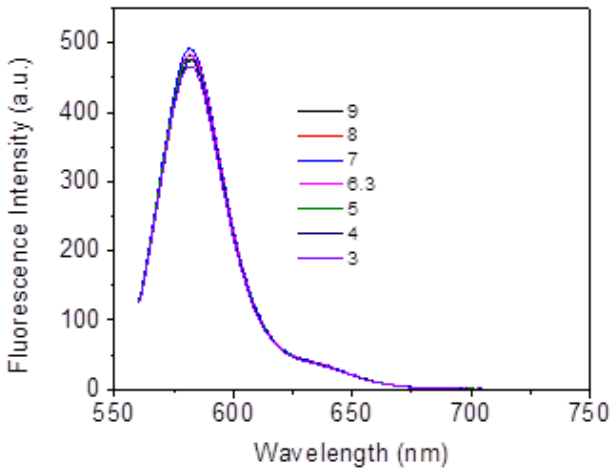

(a)

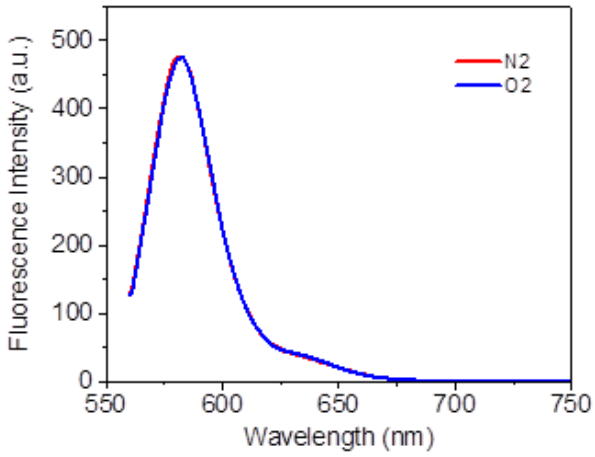

(b)

Figure 21: (a) pH responses of the built-in probe film excited at 540 nm; (b) Oxygen responses of the built-in reference probe excited at 540 nm

3.3.2 Optimization of exposure time

The exposure time is the most critical parameter in optimizing the photo-patterning process. An exposure matrix from 10 seconds to 200 seconds was used to explore the optimal exposure time for each sensors. The shape and size of the photo-polymerized

spots were used to evaluate exposure dose. Over exposure will result in larger spots and the polymerization on the non-exposed area due to diffusion of radicals in the masked area. The under exposure will result in incomplete polymerization thus leading to the smaller size of spots or peel of spots during the washing step.

It was discovered that each of the sensors has its own optimal exposure time. Typical fluorescence and bright field images, along with the spot size for each of the three sensors will be discussed.

Figure 22 shows the optimal exposure time for pH sensor is 40 seconds, while over-exposure and polymerization under the masked area is obvious when the exposure time is 80 seconds. The spot size was measured as 30.7 μm while the mask contained a 30 μm circle as shown in Figure 23.

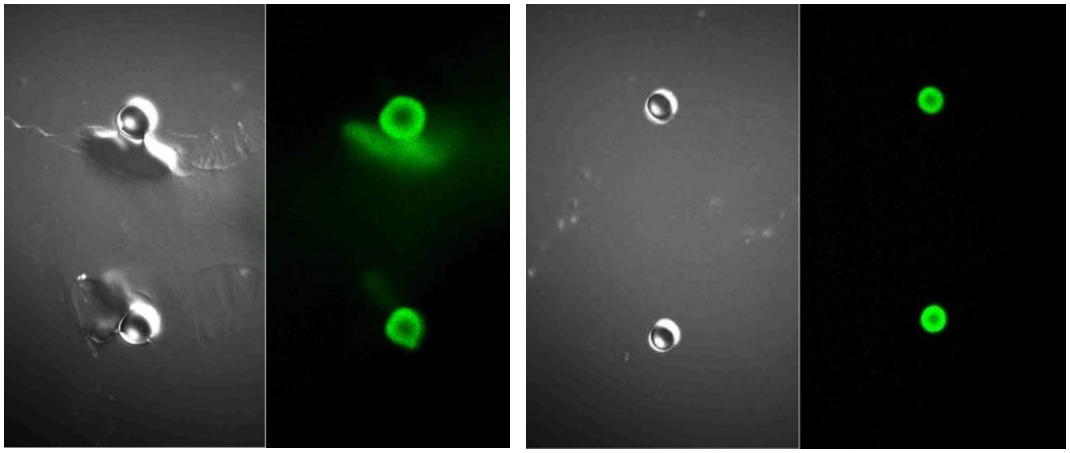

(a) (b)

Figure 22: pH sensor exposure time matrix: (a) 80s and (b) 40s

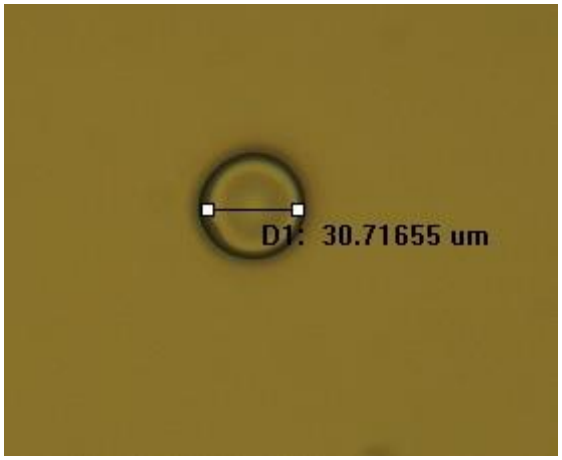

Figure 23: Bright field image of pH sensor under the optical exposure time of 40 seconds

Figure 24 shows the over exposure, the optimal exposure and the under exposure time of 150 seconds, 120 seconds and 80 seconds, respectively, for the oxygen sensors. The spot size was 30.3 µm when the optimal exposure time of 120 seconds was applied as shown in Figure 25.

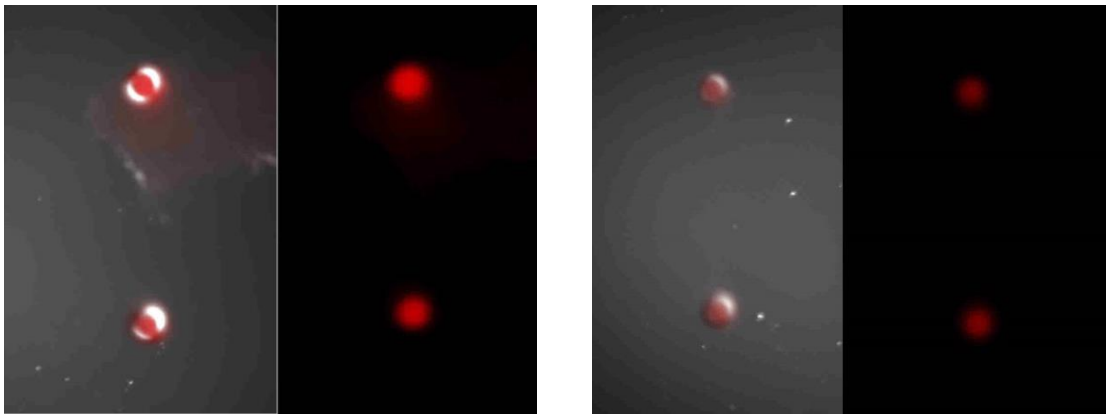

(a) (b)

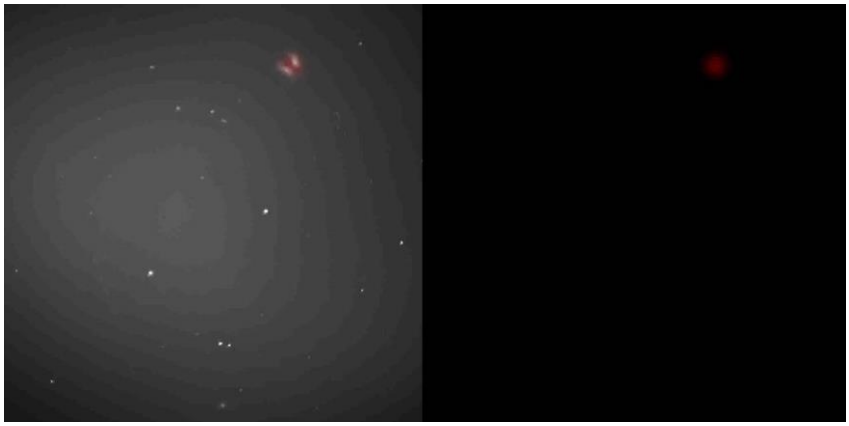

(c)

Figure 24: Oxygen sensor exposure time matrix: (a) 150s, (b) 120s and (c) 80s

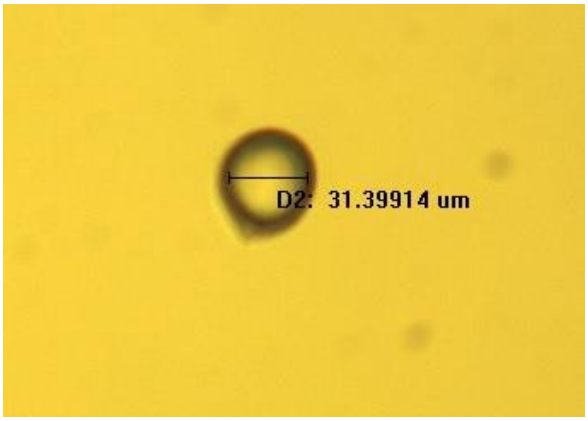

Figure 25: Bright field image of oxygen sensor under the optical exposure time of 120 seconds

Figure 26 shows the over exposure, the optimal exposure and the under exposure time of 90 seconds, 70 seconds and 30 seconds, respectively, for the Rhodamine sensors. The spot size was 30.7 μm when the optimal exposure time of 70 seconds was applied as shown in Figure 27.

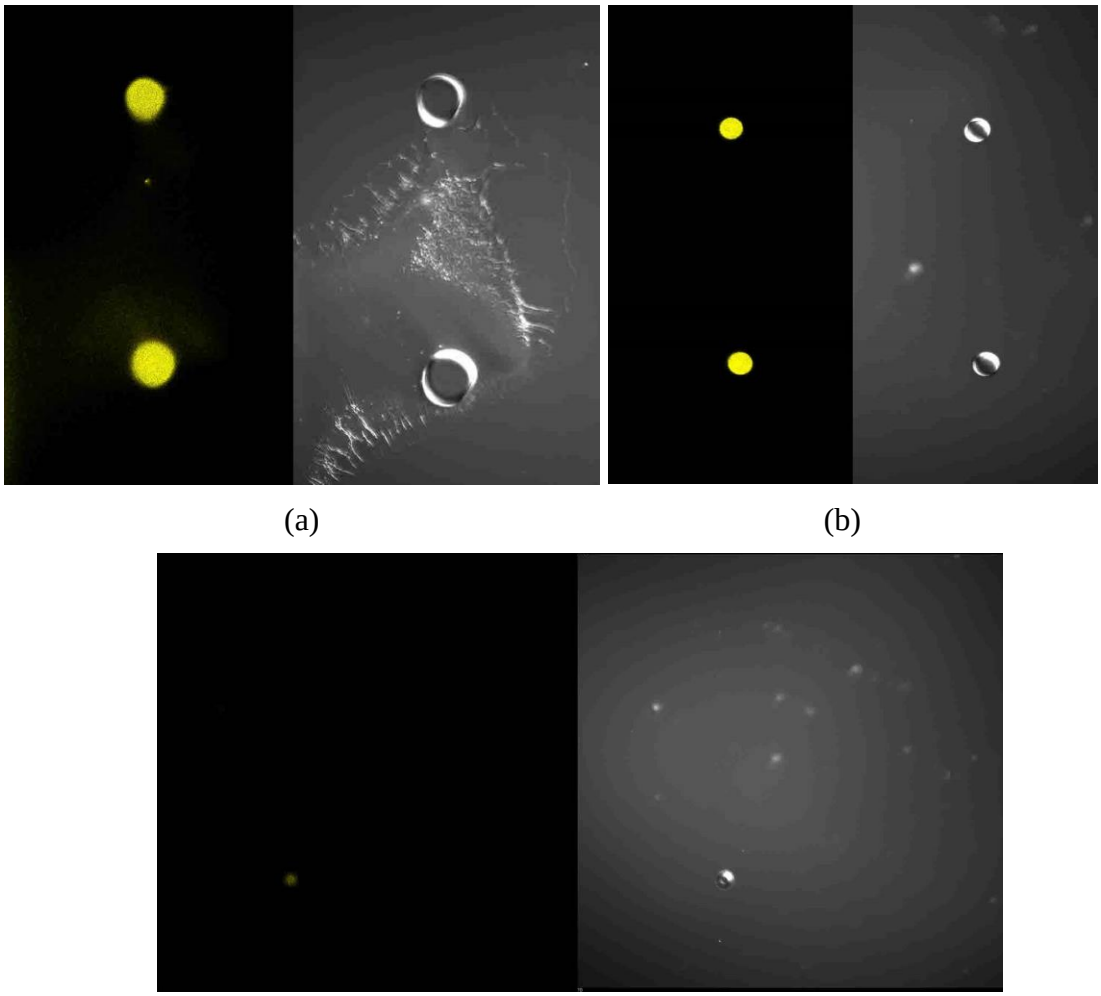

Figure 26: Rhodamine sensor exposure time matrix: (a) 90s, (b) 70s and (c) 30s

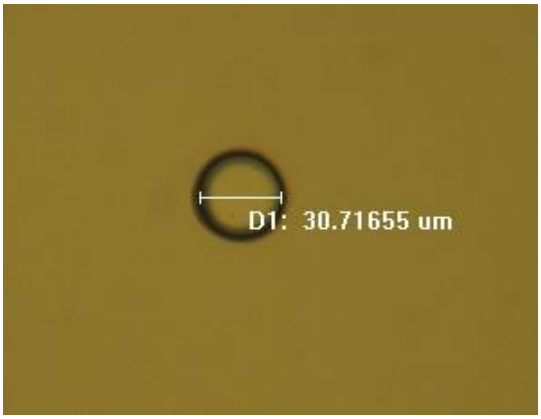

Figure 27: Bright field image of Rhodamine sensor under the optical exposure time of 70 seconds

3.3.3 Cell loading

Microwell arrays were fabricated containing lips for confinement of single cells using an HF wet etching process as detailed in Chapter 2. The pitch of the microwell array is 300 µm while the inner diameters of lips are 110 µm which match triple sensor arrays confined inside a circle of 90 µm diameter. The dies containing microwells were glued to 35 mm petri dishes for cell loading and incubation (Figure 28). CPA cells derived from Barrett's Esophagus were loaded into the microwell using a home-built piezo-driven pico-pump (Figure 29) [22].

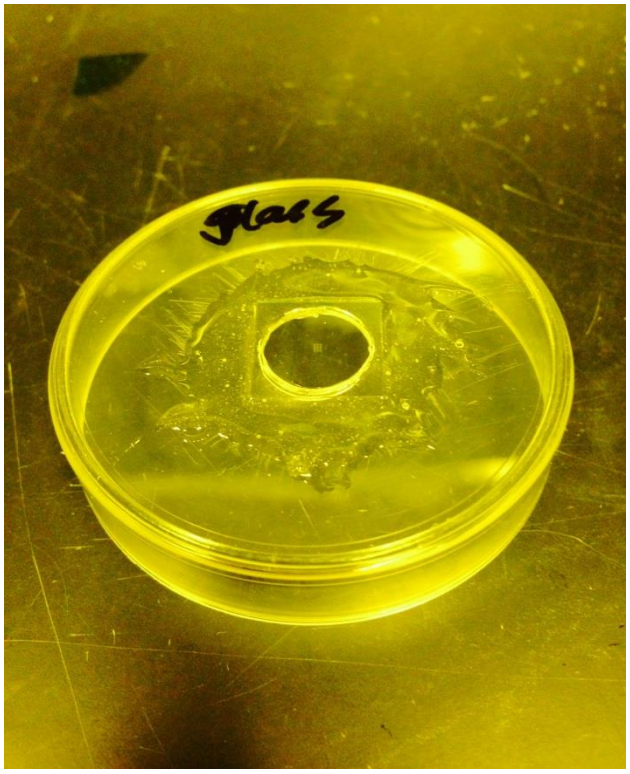

Figure 28: Petri-dish with microwells

Figure 29: Single cell loader

Microwell arrays were loaded with single cells and incubated for 24 hours. Two microwells with no cells were used as control as shown in Figure 30.

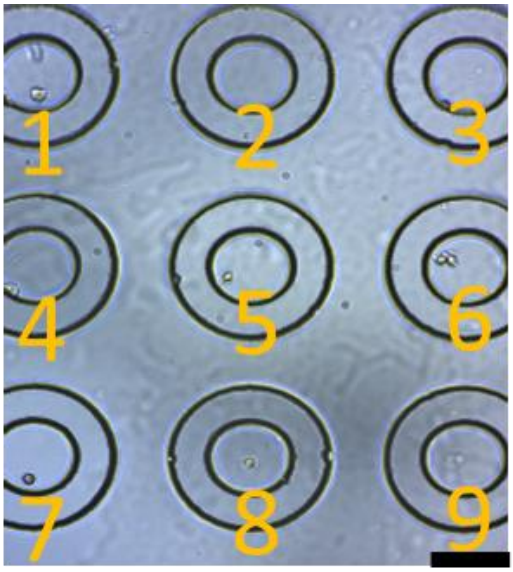

Figure 30: Microwell loaded with single cells. Scale bar: 100µm

3.3.4 Metabolic profiling

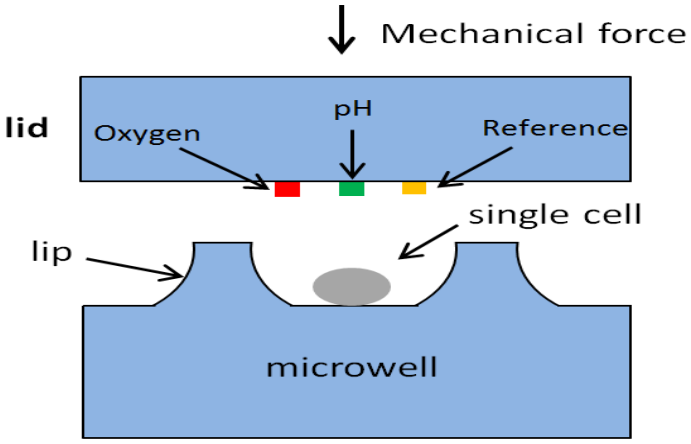

Figure 31: "Draw-down" configuration

The metabolic "draw-down" method was performed by aligning sensor arrays to the microwell arrays on a home-built "draw-down" station adapted from an inverted microscope (Figure 31) [22]. The fluorescence intensities from triple sensor arrays were automatically collected for 90 minutes at 1 minute intervals, and were plotted in Figure 32. Heterogeneous oxygen and pH responses are observed from different single cells and no response from control microwells without any cells. The reference sensors show no response, which will be used as reference in ratiometric analysis.

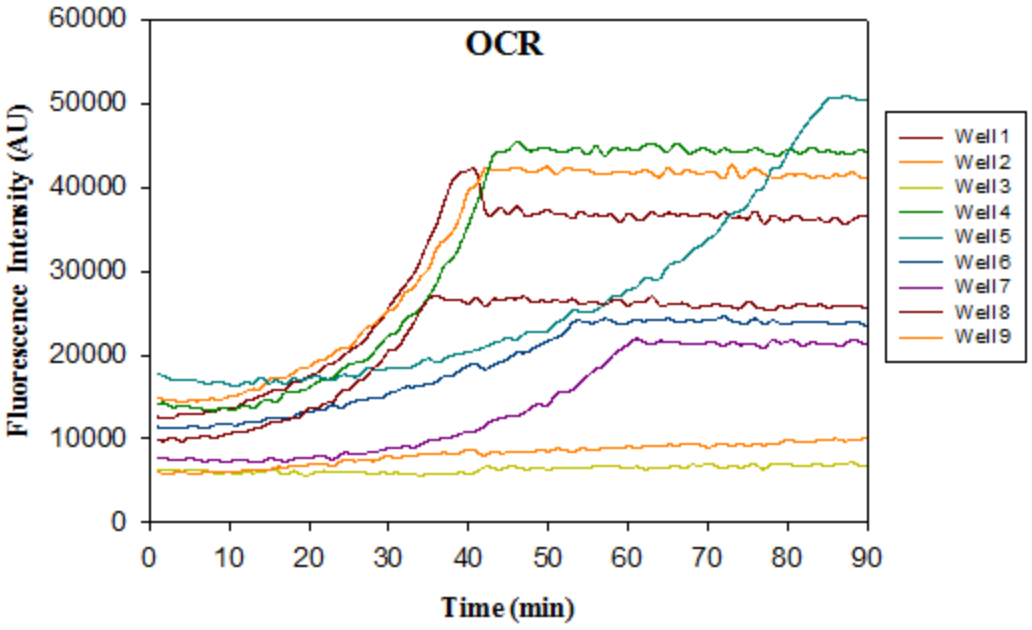
OCR
Fluorescence Intensity (AU)
60000
50000
40000
30000
20000
10000
0
0
10
20
30
40
50
60
70
80
90
Time (min)
Well1
Well2
Well3
Well4
Well5
Well6
Well7
Well8
Well9

(a)

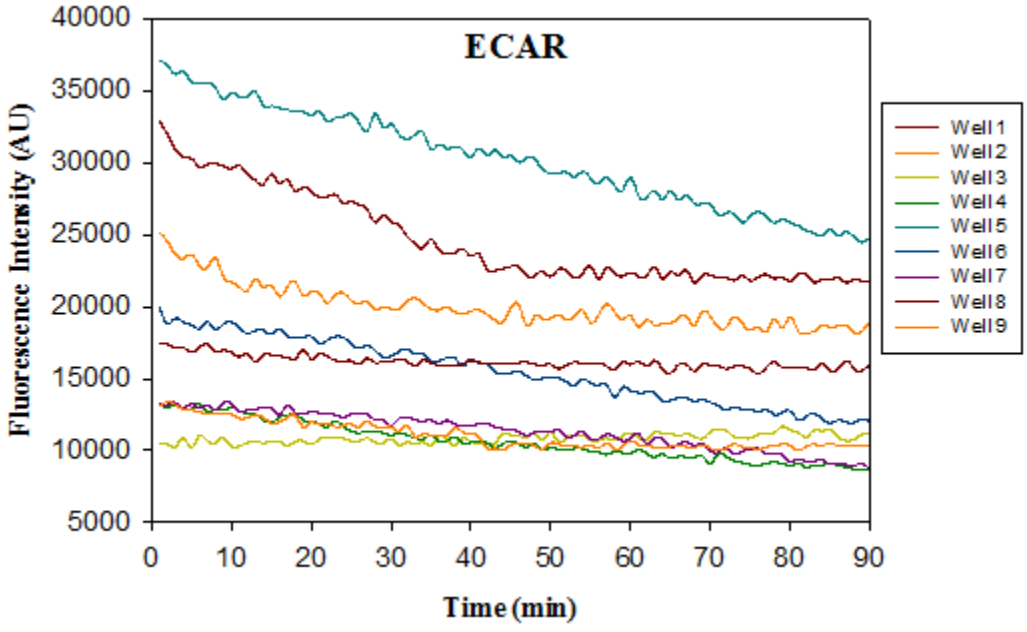
ECAR
Fluorescence Intensity (AU)
40000
35000
30000
25000
20000
15000
10000
5000
0
10
20
30
40
50
60
70
80
90
Time (min)
Well1
Well2
Well3
Well4
Well5
Well6
Well7
Well8
Well9

(b)

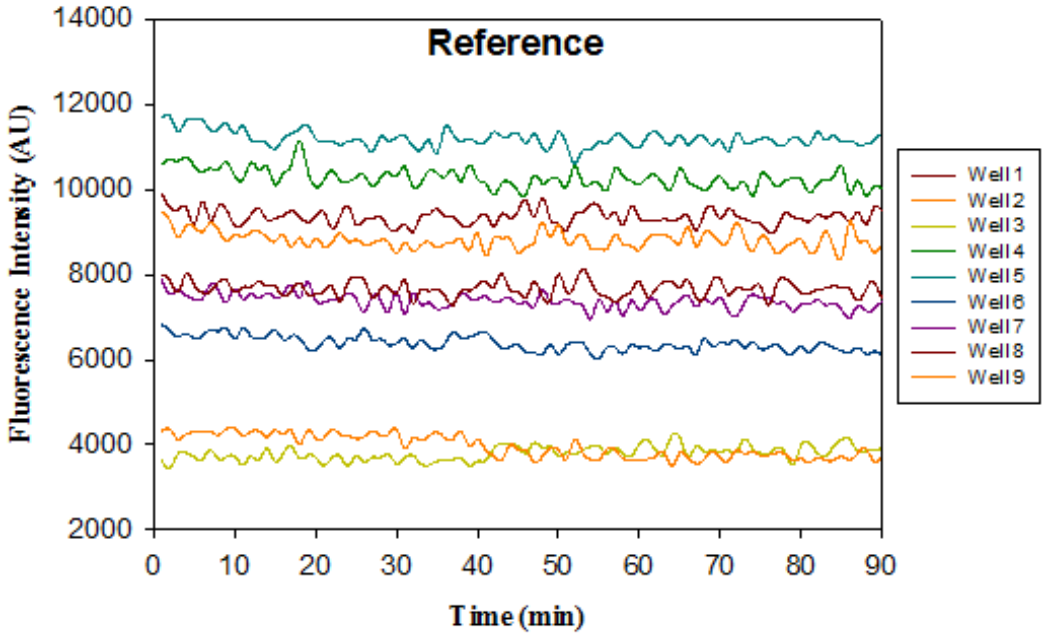

(c)

Figure 32: Single cell metabolic profiling: (a) OCR, (b) ECAR and (c) reference

3.3.5 Seal test

It is critical to prove that each of the microwells was isolated and there was no oxygen flux between one microwell to another neighbor microwell. Oxyrase was added to the culture media contained in the petri dish to deplete oxygen dissolved in the culture media. If a microwell is not completely sealed, fluorescence intensity from oxygen sensor from that microwell will increase. The seal test results from the "draw-down" in 3.3.4 are shown in Figure 33. No leaking microwell was observed.

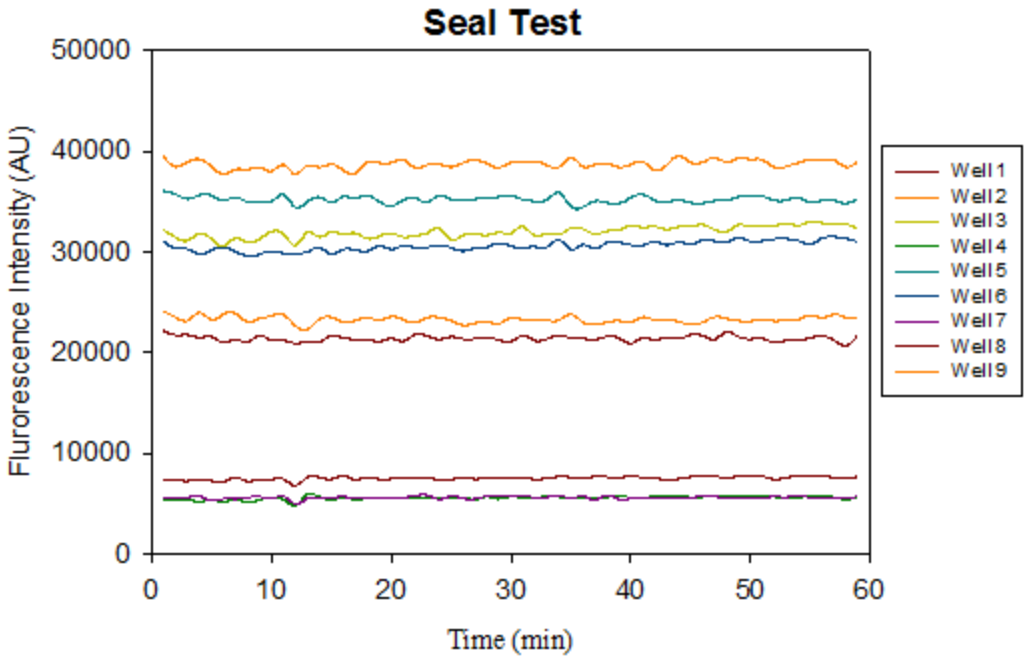

Figure 33: Seal test for "draw-down" experiment

3.4 Summary

Triple sensor arrays were patterned on fused silica chips using a three-step photo-polymerization process and oxygen and pH change were measured inside microchambers containing single live cells. The demonstration of multiple spatially resolved sensors provides a foundation for multiparameter analysis of live cell respiration and other metabolic parameters at the single-cell, multiple-cell, and tissue level.

4. PHOTO-PATTERNED, TRI-COLOR FLUORESCENCE SENSOR ARRAYS FOR SINGLE CELL MULTI-PARAMETER METABOLIC PROFILING

In Chapter 3, multi-step photo-patterning of triple sensors on a fused silica surface was successfully demonstrated. In this Chapter, the single step photo-patterning method will be used to fabricate tri-color sensors (oxygen, pH and reference) for multi-parameter metabolic profiling.

4.1 Materials and instrument

Except for the tri-color sensors, other materials and instruments used in this Chapter are the same as those in Chapter 3. The polymerizable tri-color, dual pH and oxygen sensor was synthesized by the chemistry group led by Dr. Yanqing Tian in CBDA.

4.2 Experiments

The single step photo-patterning process is the same as the photo-patterning process detailed in Chapter 3, but alignment or second/third exposure was not performed.

4.3 Results and discussions

4.3.1 Tri-color dual pH and oxygen sensor film responses

Figure 34 shows the pH and oxygen responses of the dual pH and oxygen sensor. The sensor comprises a pH probe with an emission maximum at 515 nm, an internal built-in reference probe with an emission maximum at 580 nm, and an oxygen probe with an emission maximum at 650 nm. Figure 34 A shows the pH responses of the dual sensor excited at 488 nm. The emission at 515 nm increases with the increase of pH. The emission at 580 nm also increases with the increase of pH when excited at 488 nm. This is due to a slight overlay of

the fluorescence from the pH probes with the built-in reference probes. When excited at 540 nm, the emission at 580 nm has no responses to pH (Figure 34 B). The oxygen sensor with an emission maximum at 650 nm does not respond to pH when excited at either 488 nm or 540 nm. Figure 34 C shows the pH responses of the sensor calculated by the changes of the intensities at 515 nm and also the ratiometric approach using the ratios of emission intensities at 515 nm and at 580 nm. The pH responses cover the physiological ranges from 7.5 to 5.5, indicating its applicability for biological pH measurements.

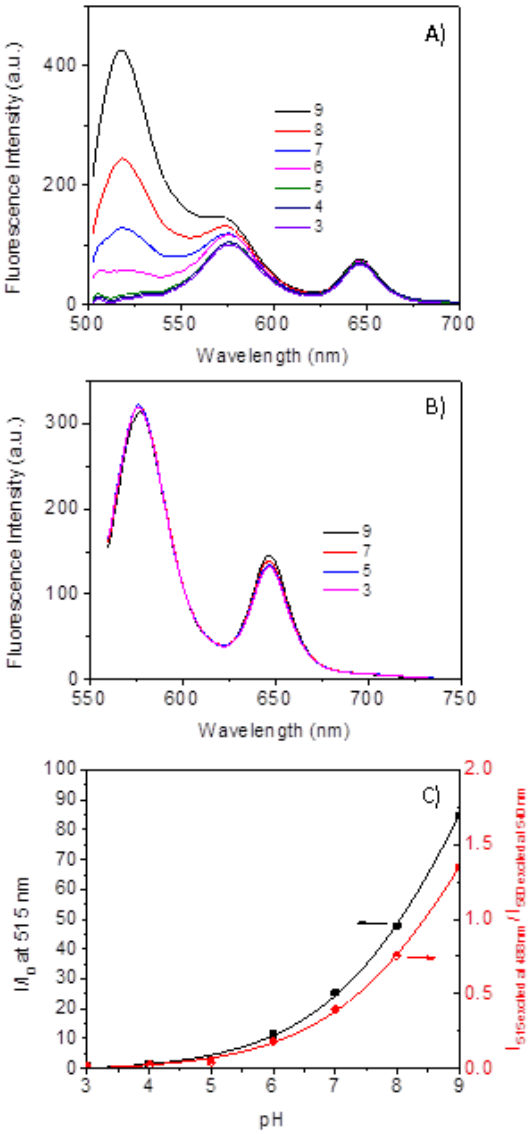

Figure 34: (A) pH responses excited at 488 nm; (B) pH responses of the reference probes and oxygen probes; (C) pH responses as measured using emission intensity at 515 nm and the ratio between intensities at 515 nm and 580 nm

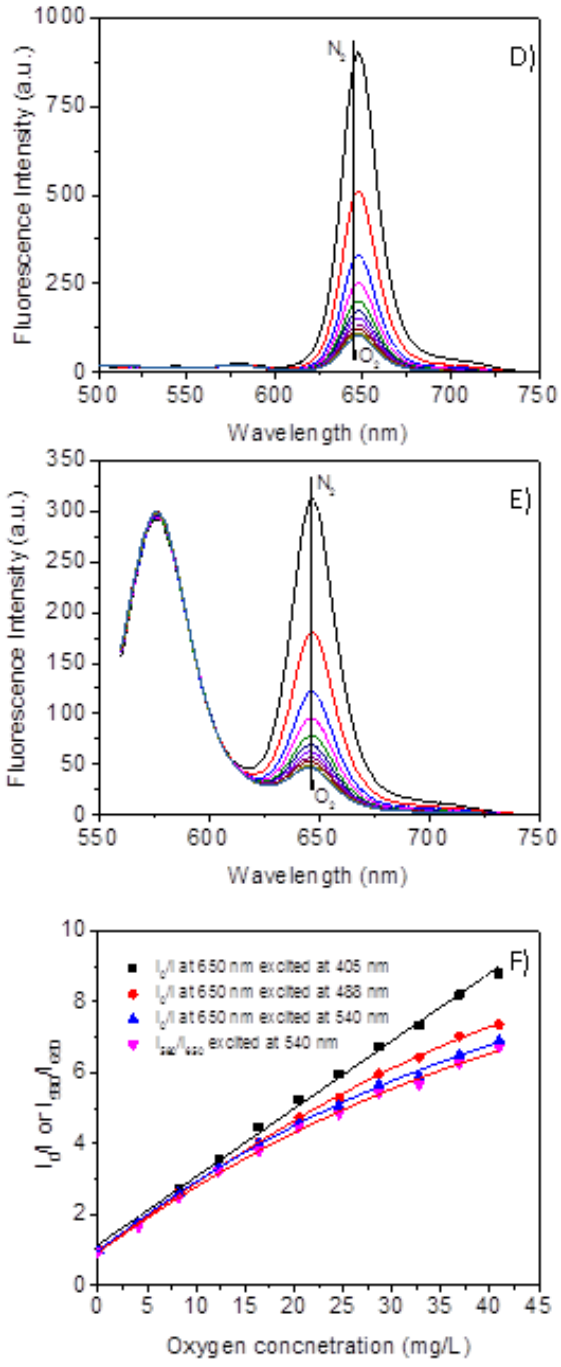

Figure 35: (D) oxygen responses excited at 405 nm; (E) oxygen responses excited at 540 nm; (F) Stern-Volmer plots of the oxygen responses using the different methods. Note dissolved oxygen in air saturated water at 23 °C is 8.6 mg/L or 8.6 ppm

Figure 35 D and E show the oxygen responses excited at 405 nm and 540 nm, respectively.

The emission intensities of the oxygen sensor increase with a decrease in dissolved oxygen concentrations, similar to other oxygen sensors. Figure 35 F shows the Stern-Volmer plots of the oxygen responses calculated using different approaches. The sensor responds linearly to oxygen when excited at 405 nm, because at such an excitation wavelength, the rhodamine derived built-in reference and pH probe were not excited efficiently. Although non-linear Stern-Volmer plots were observed when excited at other wavelengths, such as 488 and 514 nm at high oxygen concentrations, because of the slight overlay of the emissions of the built-in reference probes with the oxygen sensor's emissions, all the plots show linear responses to oxygen from deoxygenated condition to dissolved oxygen concentration of 10 mg/mL corresponding to oxygen fraction of 24% in air. The linear responses make the calculation of oxygen concentrations simple when used for cellular oxygen respiration studies.

4.3.2 Optimization of wavelengh for photo-polymerization

There are three UV wavelengths, 380 nm, 405 nm and 435 nm, available in MPS. The optimal wavelength for photo-patterning tri-color sensors was obtained with the mask shown in Figure 36.

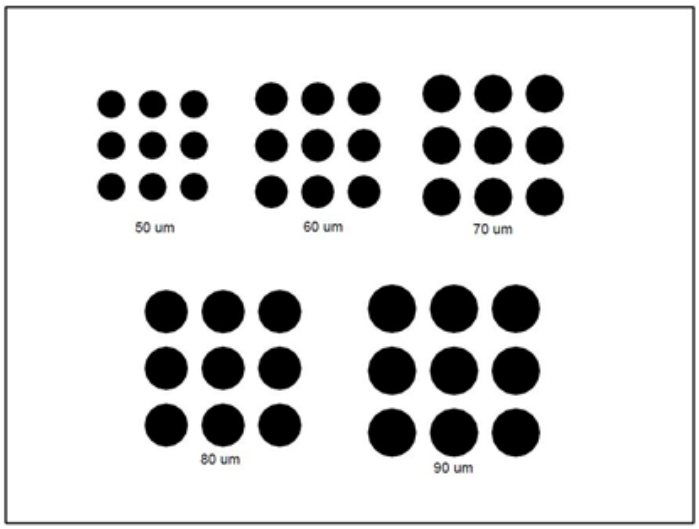

Figure 36: Virtual mask for optimizing exposure wavelength and exposure time

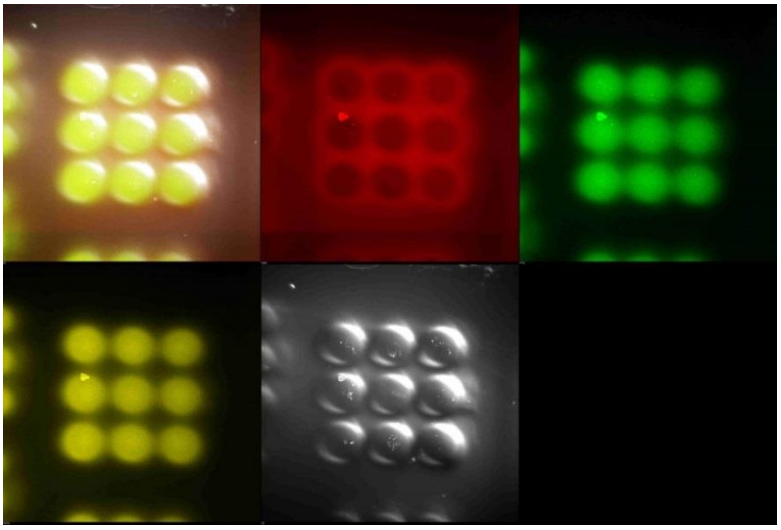

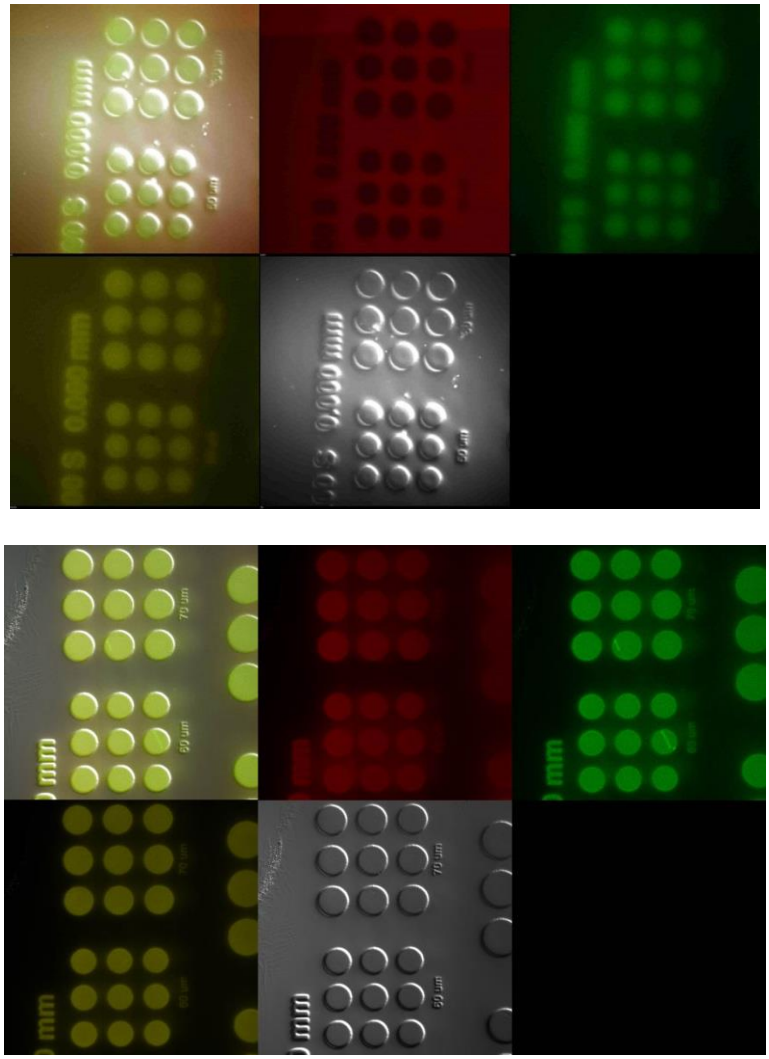

Figure 37: Fluorescence images and bright field image from tri-color sensor arrays photopolymerized by (top) 380 nm; (middle) 405 nm and (bottom) 435 nm UV

The tri-color sensor arrays photo-polymerized by 380 nm UV formed spots that seemed anomalous in shape. They have curved instead of flat top surfaces. The fluorescence emission from oxygen sensors was weaker than background fluoresence. The tri-color sensor arrays photo-polymerized by 405 nm UV showed improvement in terms of sensor shape; however fluorescence emission from oxygen sensors was still weaker than background fluoresence.

The tri-color sensor arrays photo-polymerized by 435 nm UV showed best results in terms of fluoresence intensities from pH, oxygen and reference sensors, the flat top surface and the sharp edges (Figure 37). Therefore, 435 nm UV was used to photo-pattern sensor arrays for experiments in this chapter.

4.3.3 Optimization of exposure time

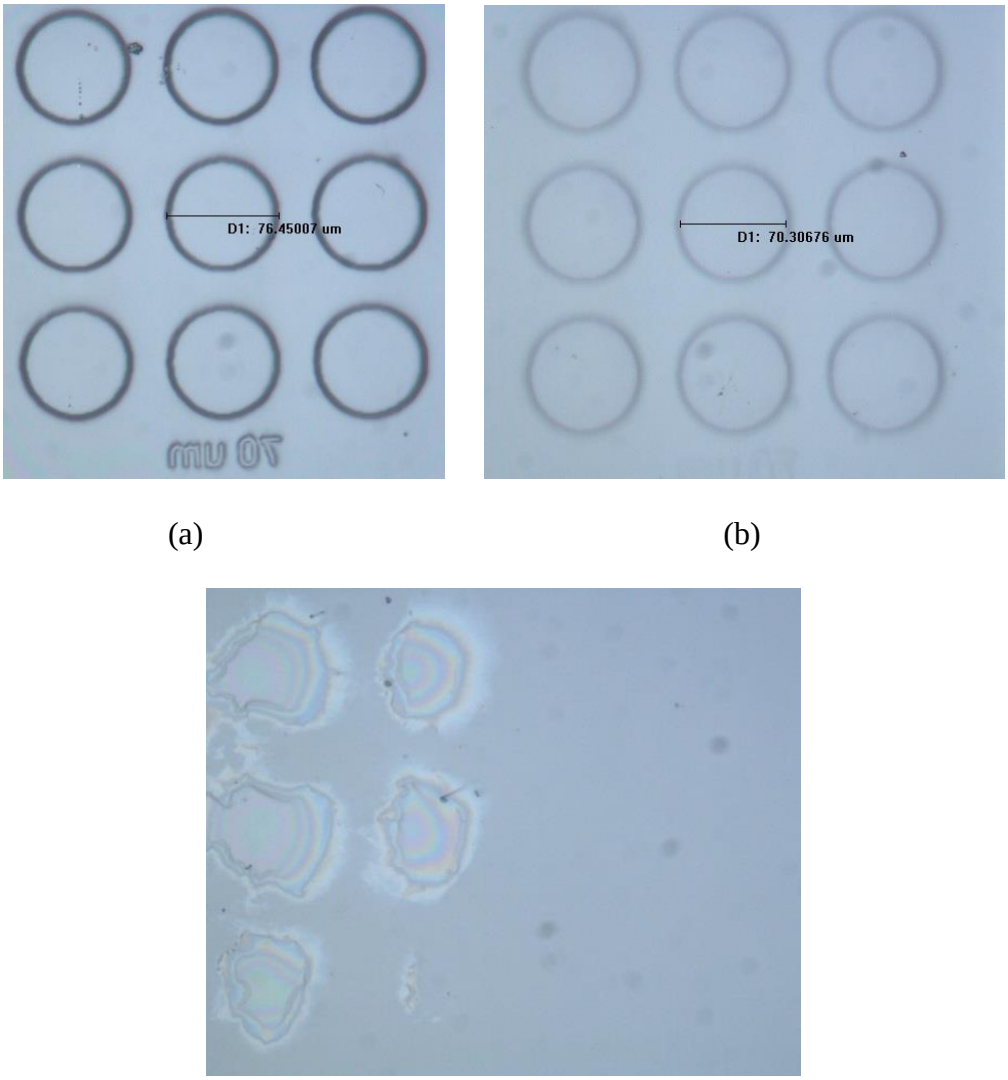

(a) (b)

(c)

Figure 38: Bright field images of tri-color sensor arrays photo-polymerized by (a) 85 seconds, (b) 70 seconds and (c) 30 seconds of 435 UV exposure

The exposure matrix and criteria used to evaluate the optimal exposure time were detailed in Chapter 3. The exposure matrix from 30 seconds to 90 second with 5 second intervals was performed. The results in Figure 38 show that 70 seconds exposure time generates 70.3 μm spots, close to the 70 μm circles designed on the visual mask.

4.3.4 Fluorescence emission spectrum from tri-color sensor arrays

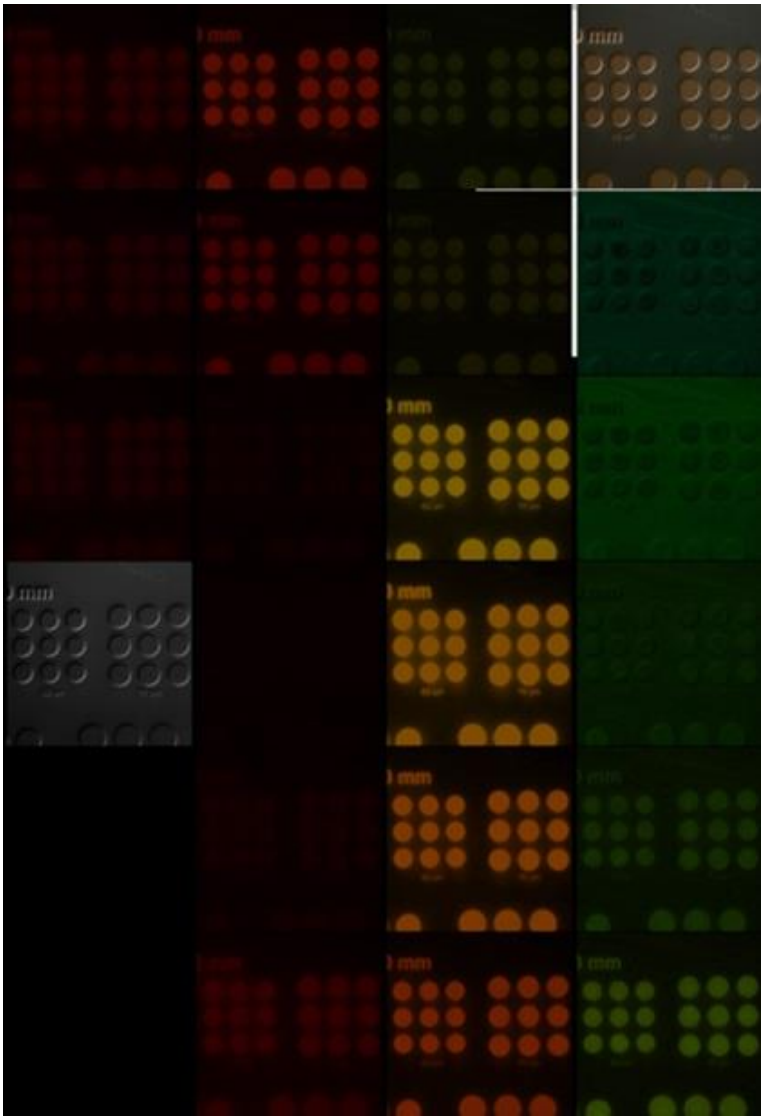

Figure 39: Fluorescence images collected from confocal spectrum scanning

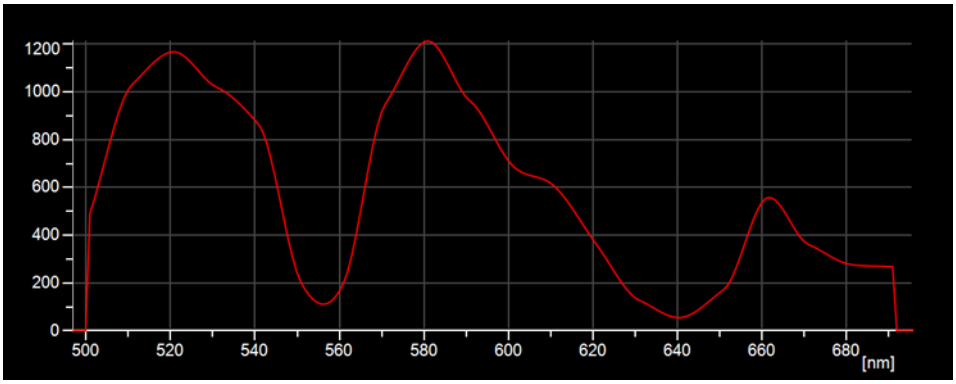

Figure 40: Fluorescence spectrum from fluoresence image series in (a)

Using the optimal exposure time of 70 seconds, a tri-color sensor array was photo-patterned and the fluorescence spectrum was analyzed using the spectrum scanning function of the Nikon confocal microscope. The fluorescence spectrum (Figure 40) obtained from a series of fluorescence images collected in Figure 39 is similar to spectrum in Figure 34, which indicates minimal photo damage to pH, oxygen and reference sensors during the photo-patterning process.

4.3.5 Cell loading, metabolic profiling and seal test

The cell loading, metabolic profiling "draw-down" method and seal test are detailed in Chapter 3. The microwell loaded with single cells was incubated for 24 hours. The bright field image and fluoresncece image from DAPI staining are shown in Figure 41.

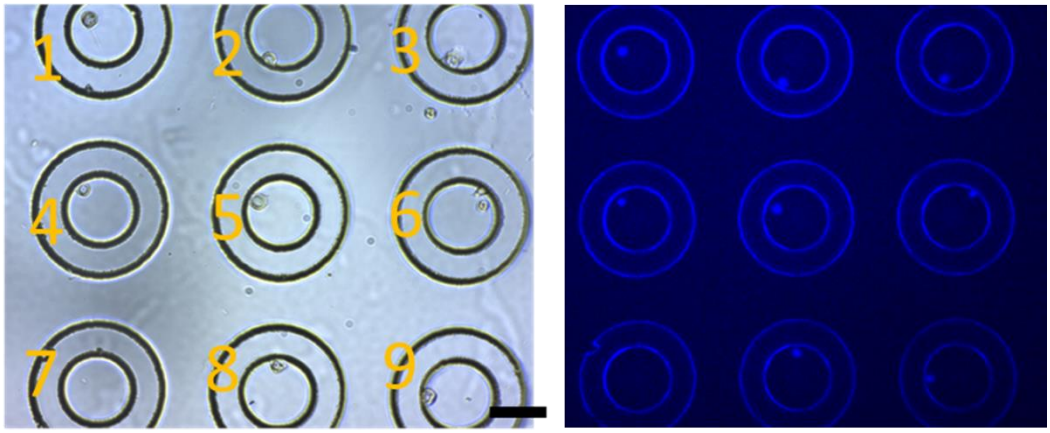

Figure 41: Brightfield and DAPI stained single cells before "draw-down"

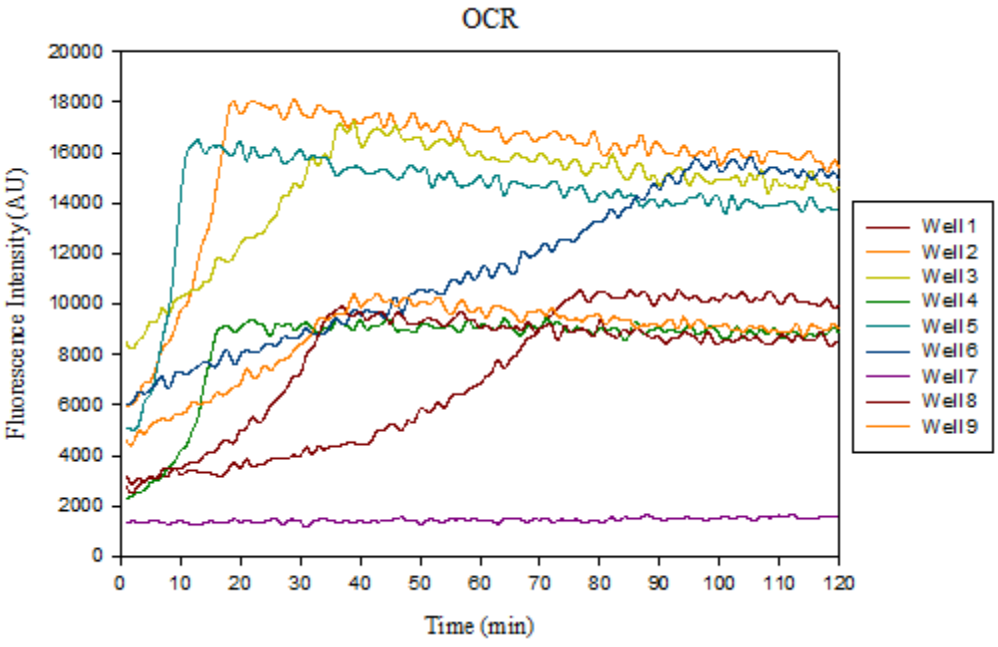

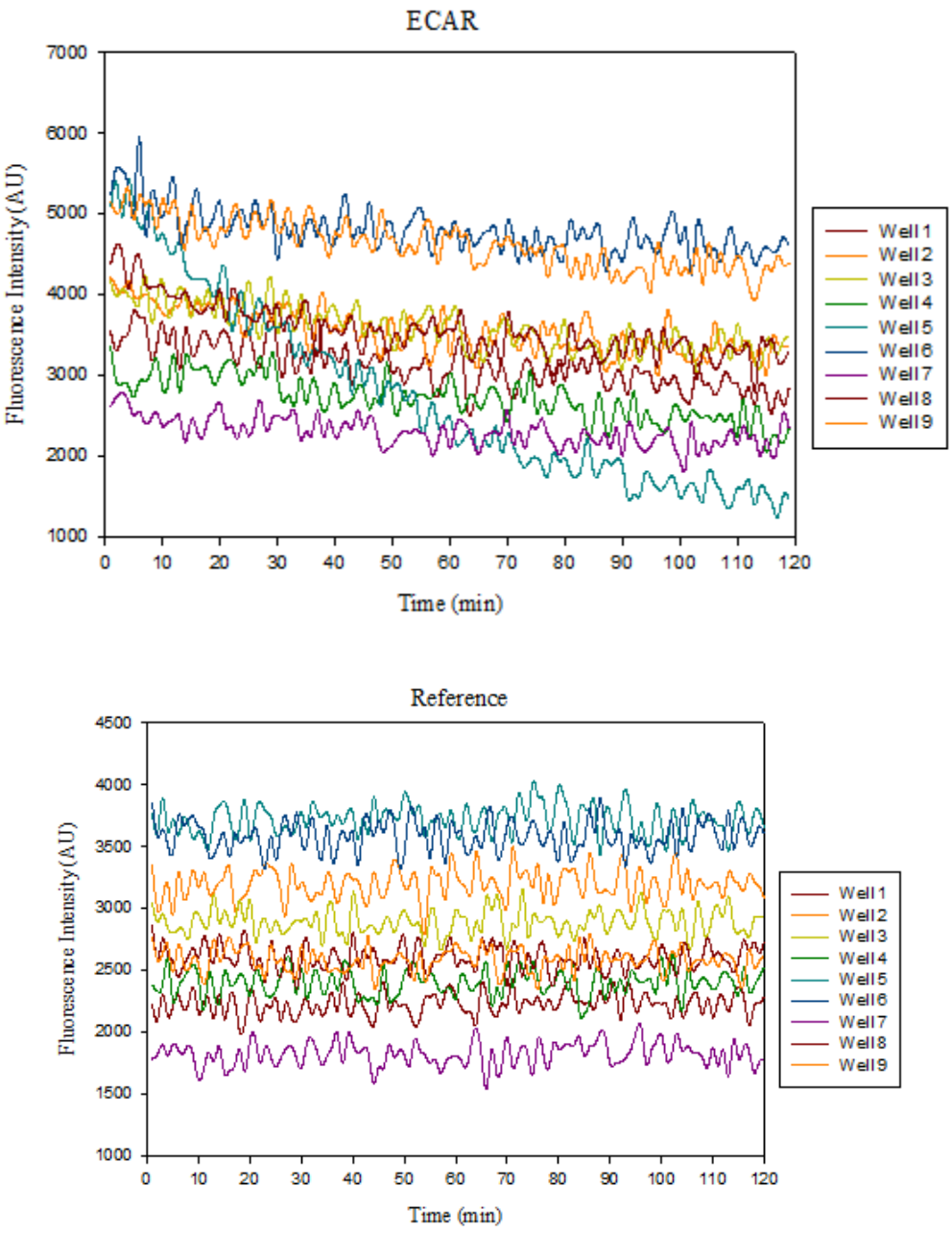

Figure 42: Fluorescence intensities from oxygen, pH and reference sensors

Figure 42 shows heterogeneous oxygen and pH responses from different single cells and no response from the control microwell 7 with no cells. The reference sensors show no response, which will be used as reference in ratiometric analysis.

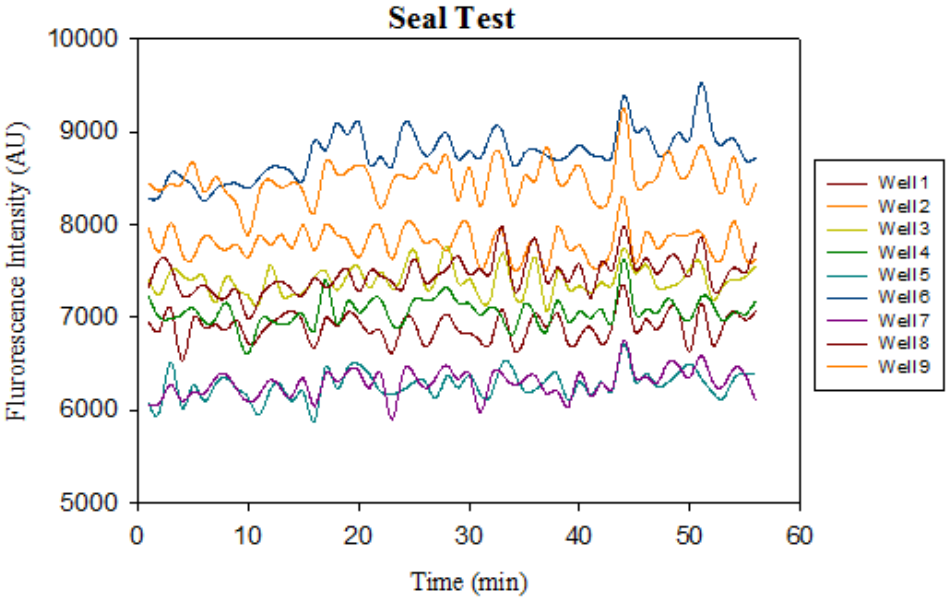

Figure 43: Seal test for "drawdown" experiment

4.4 Summary

Tricolor sensor arrays were photo-patterned on fused silica chips using a single-step photo-polymerization process and oxygen and pH changes were measured inside microchambers containing live single cells. The tri-color spectrally resolved sensor can be used in multiparameter analysis of live cell respiration and other metabolic parameters at the single-cell, multiple-cell, and tissue level.

5. SOFT MATERIAL "DRAW-DOWN"- PRELIMINARY RESULTS

Another major technical challenge in metabolic profiling using fused silica as a substrate material is that the yield of hermetic sealing between two rigid fused silica parts, even with a compliance layer of PDMS or Parylene C, is relatively low. Any particles trapped in between two fused silica parts will cause "non-seal", leading to failure of the experiment. In this chapter, "soft" materials such as KMPR negative photoresist and polyethylene terephthalate (PET) are used as a substrate to address the sealing issues.

5.1.1 KMPR/SU-8 microwells for cell loading

Compared to fused silica wet etched microwells, the advantages of SU-8/KMPR microwells include: (1) significant savings in overall processing time (~20 hours to ~10 hours) and hands-on time (~16 hours to ~ 3 hours) and (2) providing a soft material for better hermetic sealing. The adhesion of SU-8/KMPR to a substrate after prolonged exposure in cell culture media (moisture and salts) is a major challenge in SU-8/KMPR based microwells. Preliminary experiments were performed to optimize the pre-bake, post-bake and hard-bake conditions and back-side exposure techniques were used. The result is that SU-8/KMPR can withstand the harsh conditions required for single-cell metabolic analysis. Seal tests will be performed, followed by oxygen consumption rate measurements using SU-8/KMPR microwells.

5.1.2 Improved fabrication procedures

The original fabrication procedures and improved fabrication procedures are compared in Table 2.

Table 2: Detailed process flow of the original frontside and optimized backside exposure

Important steps	Original front-side exposure	Optimized backside exposure
Wafer preparation	RCA cleaning Dehydrate at 160° C for 30 minutes Surface treatment by oxygen plasma for 10 minutes at 200 W and 300 mTorr	Same
Patterned chrome layer	Not applied	100 nm Cr coating Spin speed 4500 rpm (40 seconds) for AZ 4330 Softbake: 90 seconds Exposure: 150 mJ/cm^2 AZ300MIF development Develop about 90 Rinse in DI water and dry with Nitrogen blows Patterns inspection Hardbake 110°C for 3 minutes Chrome etch for about 2 minutes AZ 4330 removal by Microstrip 2001

SU8/KMPR patterning	KMPR 1025: - Spincoat: 4000 rpm for 20 µm thickness - Softbake: 1 minute at 65° C and then an infinity (>5° C/minute) ramp to 95° C and hold for 5 minutes on a hot plate; cool to room temperature (R.T.) - Exposure: 730 mJ/cm^2 with and i-line filter - Post Exposure Bake: Ramp at infinity to 95 °C from R.T. - Develop for 5-7 minutes with agitation and inspection - Hardbake: Ramp at infinity to 150 °C	KMPR 1025: - Spin speed 4000 rpm for 20 µm thickness on chrome side - Softbake: Ramp from R.T. to 95° C and hold for 5 minutes; remove from hot plate until cooling to R.T. All ramps, applied for softbake, post exposure bake and hardbake, were set to 1°C/minute to decrease mechanical stress and improve adhesion - Exposure: 730 mJ/cm^2 with and i-line filter. The KMPR (chrome) side faced down on the OAI aligner stage - Post Exposure Bake: Ramp at 1°C/minute to 95 °C from R.T.; cool to R.T. at 1°C/minute - Develop for 5-7 minutes with agitation and inspection - Hardbake: Ramp at infinity to 150 °C from R.T.; cool to R.T. at 1°C/minute

	SU8 3025: - Spincoat: 4000 rpm for 20 µm thickness - Softbake: 1 minute at 65° C and then an infinity (>5° C/minute) ramp to 95° C and hold for 10 minutes on a hot plate; cool to room temperature (R.T.) - Exposure: 225 mJ/cm^2 with and i-line filter - Post Exposure Bake: Ramp at infinity to 95 °C from R.T. - Develop for 4-5 minutes with agitation and inspection - Hardbake: Ramp at infinity to 150 °C.	SU8 3025: - Spin speed 4000 rpm for 20 µm thickness on chrome side - Softbake: Ramp from R.T. to 95° C and hold for 5 minutes; remove from hot plate until cooling to R.T. All ramps, applied for softbake, post exposure bake and harkbake, were set to 1°C/minute - Exposure: 225 mJ/cm^2 with and i-line filter. The SU8 (chrome) side faced down on the OAI aligner stage - Post Exposure Bake: Ramp at 1°C/minute to 95 °C from R.T.; cool to R.T. at 1°C/minute - Develop for 4-5 minutes with agitation and inspection - Hardbake: Ramp at infinity to 150 °C from R.T.; cool to R.T. at 1°C/minute
Chrome etch	Not applied	- Chrome etch for about 2 minutes

Figure 44 shows KMPR microwells fabricated by improved fabrication procedures could survive harsh cell culture conditions for at least 48 hours.

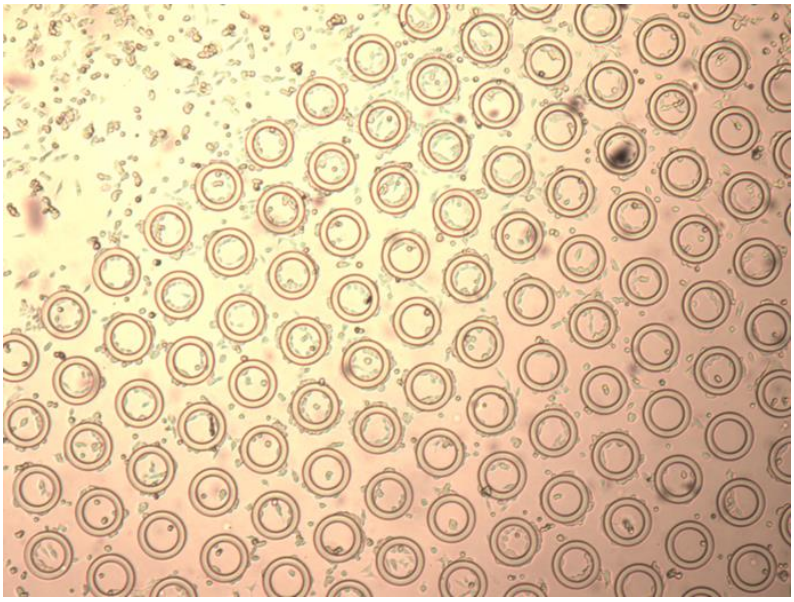

Figure 44: KMPR microwells in cell culture condition for 48 hours

5.1.3 Cell loading, metabolic profiling and seal test

The cell loading, metabolic profiling "draw-down" method, and seal test are detailed in Chapter 3. The microwell loaded with single cells was incubated for 24 hours before metabolic profiling.

The microwells loaded with single cells are shown in Figure 45. The metabolic profiling results are shown in Figure 46. The preliminary results indicated good oxygen and pH responses, as well as a good seal.

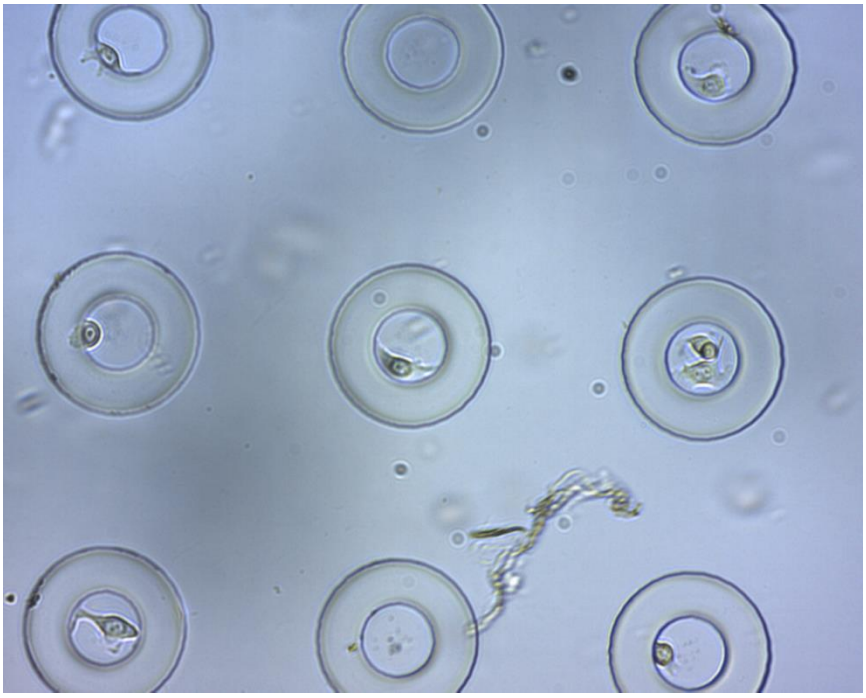

Figure 45: Cell loading in KMPR microwells

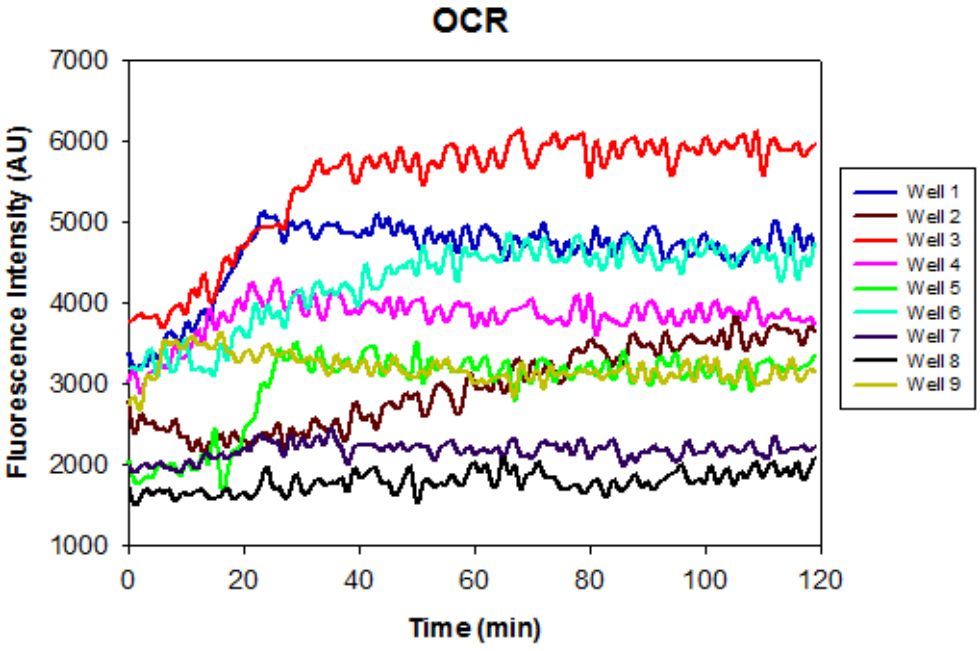

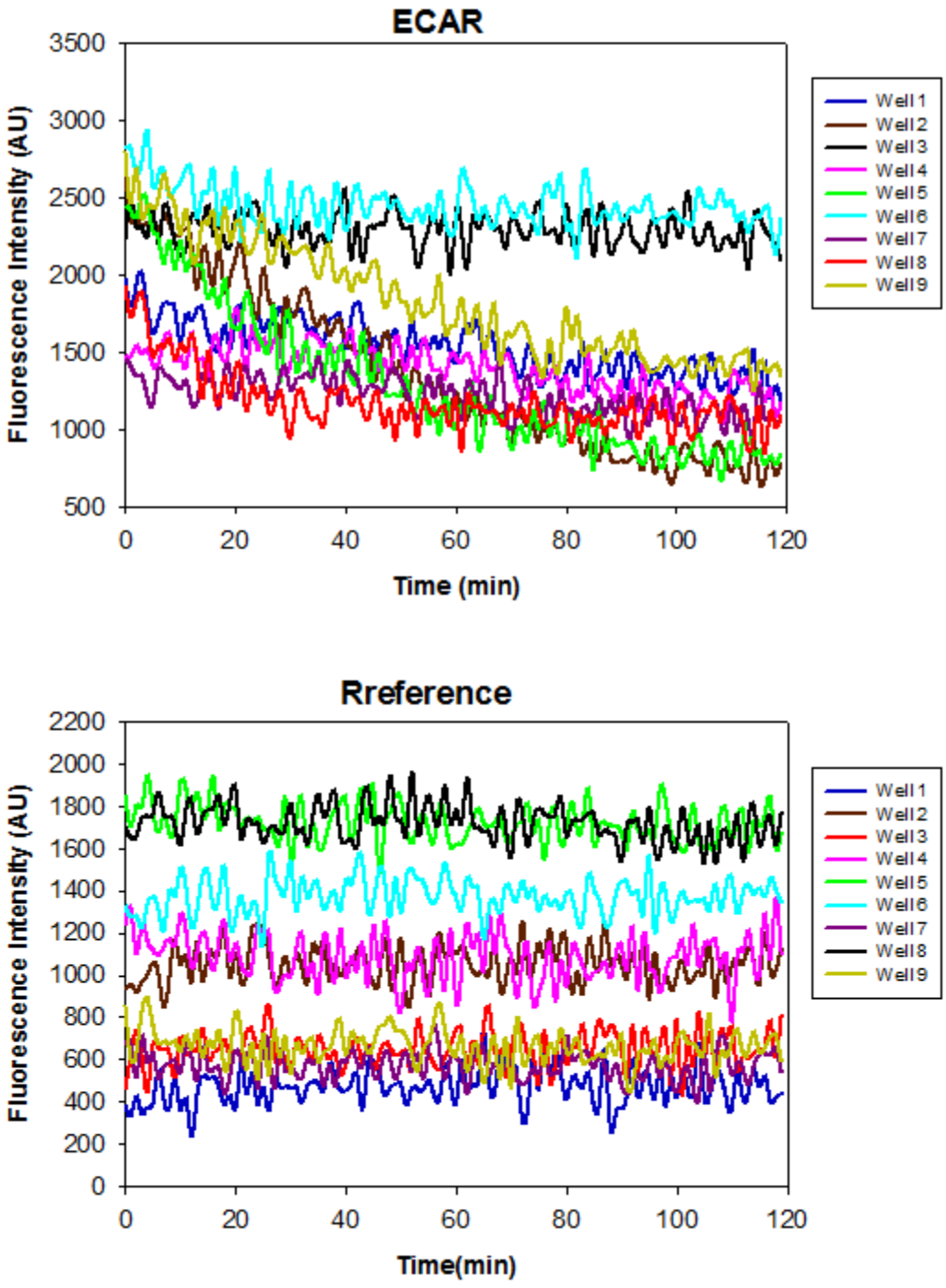

Figure 46: Single cell metabolic profiling by KMPR wells

5.2 Tri-color sensor patterning on PET

PET is another promising material with low oxygen permeability. The surface of PET was activated and functionalized using the same protocol as was used to process the fused silica substrate.

The microwells loaded with single cells are shown in Figure 47. After draw-down, the microwell lips were imprinted on the PET surface. The metabolic profiling results are shown in Figure 48 and confirm a good seal.

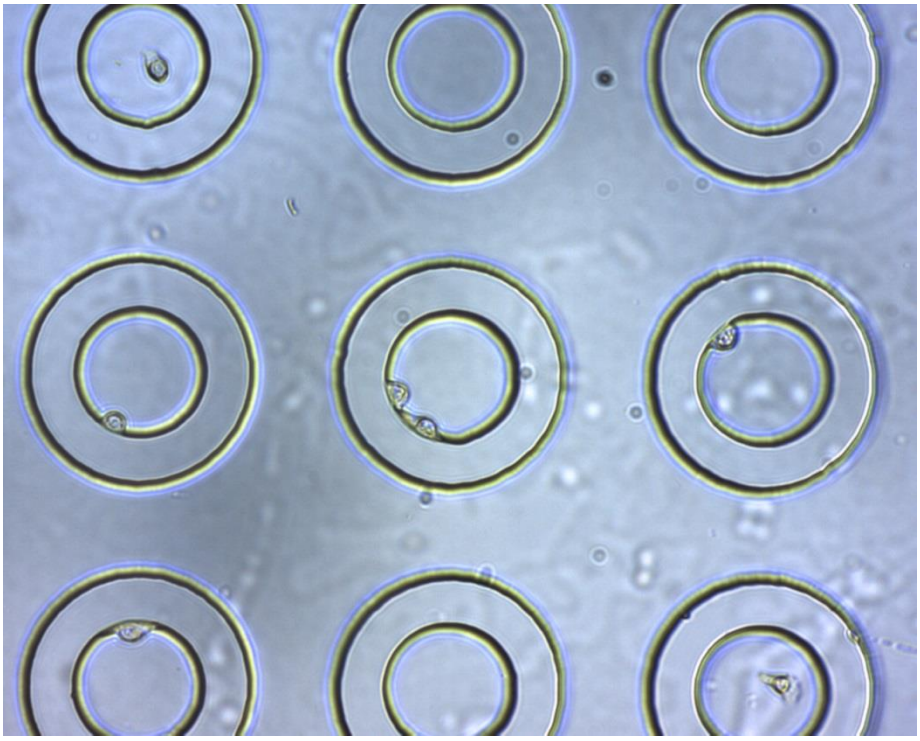

Figure 47: Cell loaded in glass microwells for sensors on PET

Fast responses and unusually slow responses were observed from different microwells in the same “draw-down” experiments as shown in Figure 48. Data is still being collected to explain the unusual responses.

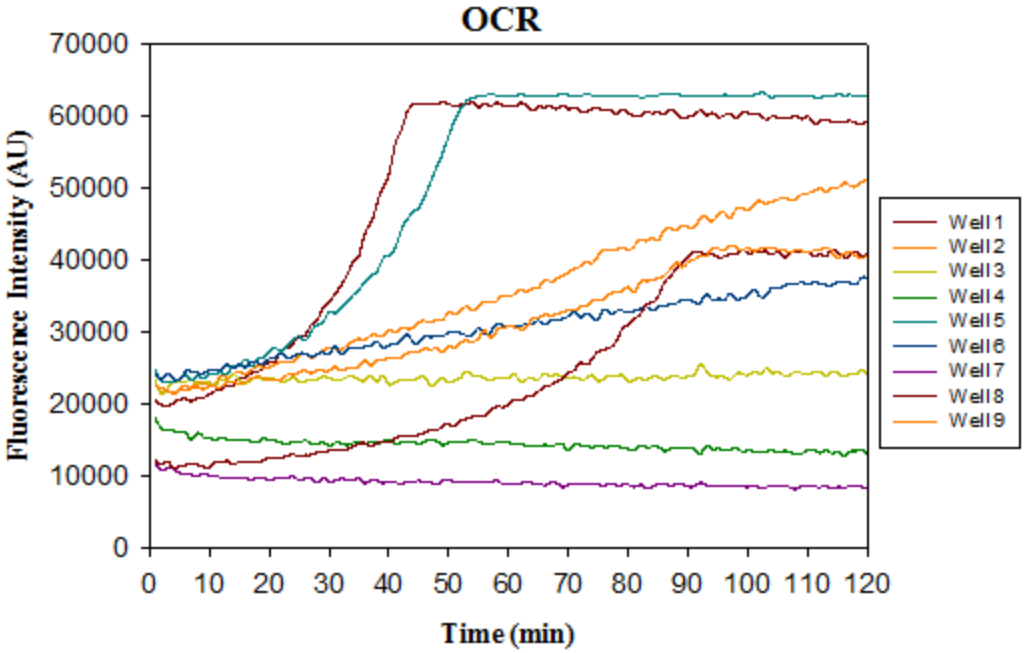
OCR
Fluorescence Intensity (AU)
70000
60000
50000
40000
30000
20000
10000
0
0 10 20 30 40 50 60 70 80 90 100 110 120
Time (min)
Well 1
Well 2
Well 3
Well 4
Well 5
Well 6
Well 7
Well 8
Well 9

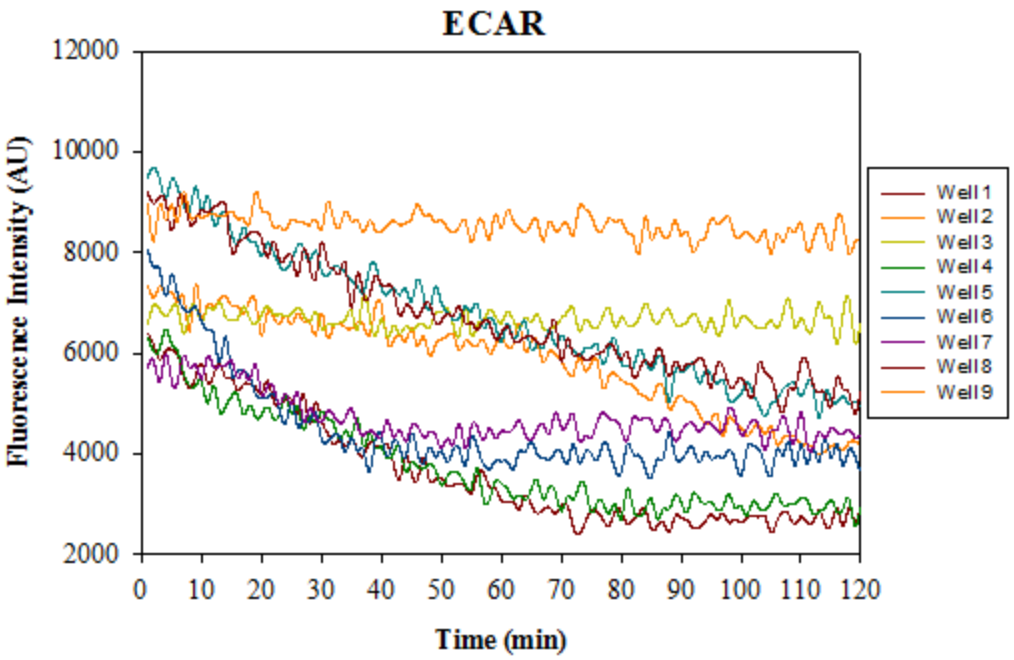
ECAR
Fluorescence Intensity (AU)
12000
10000
8000
6000
4000
2000
0 10 20 30 40 50 60 70 80 90 100 110 120
Time (min)
Well 1
Well 2
Well 3
Well 4
Well 5
Well 6
Well 7
Well 8
Well 9

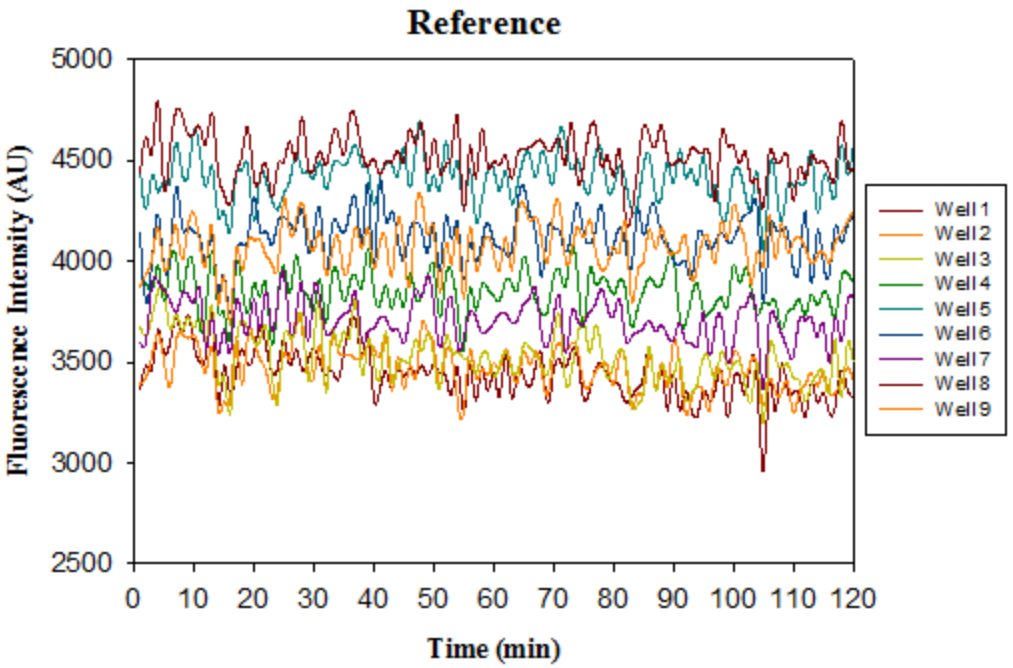

Figure 48: Single cell metabolic profiling by sensors on PET

6. SUMMARY AND FUTURE WORK

6.1 Summary of work completed

The research summarized in this thesis addresses the challenges in current single cell multi-parameter metabolic profiling by improved microfabrication enabling technologies.

In Chapter 2, the design and fabrication was described for MST lid arrays on a fused silica substrate for accommodating multiple sensors for multiparameter metabolic analysis. Two-step photolithography and wet etching processes were successfully applied to fabricate dual depth microstructures with high uniformity and low surface roughness. This work demonstrated the capability of fabricating multiple spatially resolved sensors by physically confining them inside micro-pockets before polymerization.

In Chapter 3, triple sensor arrays were patterned on fused silica chips using a three-step photo-polymerization process. The optimal exposure times for photo-polymerizing each of those three sensors were determined. The pH and oxygen responses of the sensors were characterized. The performance of the triple sensor arrays in metabolic profiling "draw-down" experiments was demonstrated.

In Chapter 4, tricolor sensor arrays were photo-patterned on fused silica chips using a single-step photo-polymerization process. The optimal exposure wavelength and exposure time were determined. The fluorescence emission spectrum was collected using a confocal microscope operated in spectrum scanning mode. The performance of the tri-color sensor arrays in metabolic profiling "draw-down" experiments was demonstrated.

The demonstration of these improved microfabrication technologies and sensors provides a foundation for multiparameter analysis of cell respiration and other metabolic parameters at the single-cell, multiple-cell, and tissue level.

6.2 Future work

Future research will focus on greater multiplexing capability and high throughput production of metabolic sensor arrays.

The spatially resolved technologies, e.g. MST micro-pocket lids and triple sensor arrays, could be combined with spectrally resolved technologies, e.g. tri-color sensor arrays to provide greater multiplexing capability.

Another direction is to improve the scale of sensor arrays from 3 x 3 spots to thousands of spots, which may require the transfer of the exposure system from a SF-100 maskless photolithography system to a UV aligner. SF-100 provides flexibility in the initial stage of technology development, however, the limited exposure area of 1 mm x 1.4 mm in a single shot and extended exposure time of several tens of seconds are not feasible to produce centimeter square arrays used in high-throughput assays.

REFERENCES

[1] J. A. Papin, N. D. Price, S. J. Wiback, D. A. Fell, and B. O. Palsson, "Metabolic pathways in the post-genome era," *Trends in Biochemical Sciences*, vol. 28, no. 5, pp. 250–258, May 2003.

[2] A. Carracedo, L. C. Cantley, and P. P. Pandolfi, "Cancer metabolism: fatty acid oxidation in the limelight," *Nat Rev Cancer*, vol. 13, no. 4, pp. 227–232, Apr. 2013.

[3] L. M. R. Ferreira, "Cancer metabolism: The Warburg effect today," *Experimental and Molecular Pathology*, vol. 89, no. 3, pp. 372–380, Dec. 2010.

[4] R. A. Cairns, I. Harris, S. McCracken, and T. W. Mak, "Cancer Cell Metabolism," *Cold Spring Harb Symp Quant Biol*, vol. 76, pp. 299–311, Jan. 2011.

[5] M. E. Lidstrom and M. C. Konopka, "The role of physiological heterogeneity in microbial population behavior," *Nat Chem Biol*, vol. 6, no. 10, pp. 705–712, Oct. 2010.

[6] D. R. Meldrum and M. R. Holl, "Microscale Bioanalytical Systems," *Science*, vol. 297, no. 5584, pp. 1197–1198, Aug. 2002.

[7] A. Raj and A. van Oudenaarden, "Nature, Nurture, or Chance: Stochastic Gene Expression and Its Consequences," *Cell*, vol. 135, no. 2, pp. 216–226, Oct. 2008.

[8] M. B. Elowitz, A. J. Levine, E. D. Siggia, and P. S. Swain, "Stochastic Gene Expression in a Single Cell," *Science*, vol. 297, no. 5584, pp. 1183–1186, Aug. 2002.

[9] J. M. Irish, N. Kotecha, and G. P. Nolan, "Mapping normal and cancer cell signalling networks: towards single-cell proteomics," *Nat Rev Cancer*, vol. 6, no. 2, pp. 146–155, Feb. 2006.

[10] R. Losick and C. Desplan, "Stochasticity and Cell Fate," *Science*, vol. 320, no. 5872, pp. 65–68, Apr. 2008.

[11] A. R. Wheeler, W. R. Throndset, R. J. Whelan, A. M. Leach, R. N. Zare, Y. H. Liao, K. Farrell, I. D. Manger, and A. Daridon, "Microfluidic Device for Single-Cell Analysis," *Anal. Chem.*, vol. 75, no. 14, pp. 3581–3586, Jul. 2003.

[12] T.-C. Chao and A. Ros, "Microfluidic single-cell analysis of intracellular compounds," *J. R. Soc. Interface*, vol. 5, no. Suppl 2, pp. S139–S150, Oct. 2008.

[13] K. Hakkila, M. Maksimow, A. Rosengren, M. Karp, and M. Virta, "Monitoring promoter activity in a single bacterial cell by using green and red fluorescent proteins," *Journal of Microbiological Methods*, vol. 54, no. 1, pp. 75–79, Jul. 2003.

[14] W. Torres-García, S. Ashili, L. Kelbauskas, R. H. Johnson, W. Zhang, G. C. Runger, and D. R. Meldrum, "A statistical framework for multiparameter analysis at the single-cell level," *Molecular BioSystems*, vol. 8, no. 3, p. 804, 2012.

[15] B. F. Brehm-Stecher and E. A. Johnson, "Single-Cell Microbiology: Tools, Technologies, and Applications," *Microbiol. Mol. Biol. Rev.*, vol. 68, no. 3, pp. 538–559, Sep. 2004.

[16] M. Russu, N. Jula, and G. Marina, "THEORETHICAL AND PRACTICAL ISSUES UPON EVOLUTION OF MICROTECHNOLOGY TOWARDS NANOTECHNOLOGY," *Moldavian Journal of the Physical Sciences*, 1950.

[17] M. E. Lidstrom and D. R. Meldrum, "Life-on-a-chip," *Nat Rev Micro*, vol. 1, no. 2, pp. 158–164, Nov. 2003.

[18] S. C. Terry, J. H. Jerman, and J. B. Angell, "A gas chromatographic air analyzer fabricated on a silicon wafer," *IEEE Transactions on Electron Devices*, vol. 26, no. 12, pp. 1880–1886, Dec. 1979.

[19] C. Cane, I. Gracia, A. Merlos, M. Lozano, E. Lora-Tamayo, and J. Esteve, "Compatibility of ISFET and CMOS technologies for smart sensors," in *, 1991 International Conference on Solid-State Sensors and Actuators, 1991. Digest of Technical Papers, TRANSDUCERS '91*, 1991, pp. 225–228.

[20] A. Manz, N. Graber, and H. M. Widmer, "Miniaturized total chemical analysis systems: A novel concept for chemical sensing," *Sensors and Actuators B: Chemical*, vol. 1, no. 1–6, pp. 244–248, Jan. 1990.

[21] T. W. Molter, S. C. McQuaide, M. T. Suchorolski, T. J. Strovas, L. W. Burgess, D. R. Meldrum, and M. E. Lidstrom, "A microwell array device capable of measuring single-cell oxygen consumption rates," *Sensors and Actuators B: Chemical*, vol. 135, no. 2, pp. 678–686, Jan. 2009.

[22] L. Kelbauskas, S. P. Ashili, J. Houkal, D. Smith, A. Mohammadreza, K. B. Lee, J. Forrester, A. Kumar, Y. H. Anis, T. G. Paulson, C. A. Youngbull, Y. Tian, M. R. Holl, R. H. Johnson, and D. R. Meldrum, "Method for physiologic phenotype characterization at the single-cell level in non-interacting and interacting cells," *J. Biomed. Opt*, vol. 17, no. 3, pp. 0370081–03700812, 2012.

[23] T. Ray, H. Zhu, and D. R. Meldrum, “Deep reactive ion etching of fused silica using a single-coated soft mask layer for bio-analytical applications,” *J. Micromech. Microeng.*, vol. 20, no. 9, p. 097002, Sep. 2010.

[24] Y. Tian, E. Fuller, S. Klug, F. Lee, F. Su, L. Zhang, S. Chao, and D. R. Meldrum, “A fluorescent colorimetric pH sensor and the influences of matrices on sensing performances,” *Sensors and Actuators B: Chemical*, vol. 188, pp. 1–10, Nov. 2013.